J. Fluid. Mech. (1994), vol. 261, pp. 95–134

Direct simulation of initial value problems for the motion of solid bodies in a Newtonian fluid Part 1. Sedimentation

By J. FENG,[1] H. H. HU[2] AND D. D. JOSEPH[1]

[1] Department of Aerospace Engineering and Mechanics and the Minnesota Supercomputer Institute, University of Minnesota, Minneapolis, MN 55455, USA

[2] Department of Mechanical Engineering and Applied Mechanics, University of Pennsylvania, Philadelphia, PA 19104-6315, USA

(Received 2 May 1993 and in revised form 23 August 1993)

This paper reports the result of direct simulations of fluid–particle motions in two dimensions. We solve the initial value problem for the sedimentation of circular and elliptical particles in a vertical channel. The fluid motion is computed from the Navier–Stokes equations for moderate Reynolds numbers in the hundreds. The particles are moved according to the equations of motion of a rigid body under the action of gravity and hydrodynamic forces arising from the motion of the fluid. The solutions are as exact as our finite-element calculations will allow. As the Reynolds number is increased to 600, a circular particle can be said to experience five different regimes of motion: steady motion with and without overshoot and weak, strong and irregular oscillations. An elliptic particle always turn its long axis perpendicular to the fall, and drifts to the centreline of the channel during sedimentation. Steady drift, damped oscillation and periodic oscillation of the particle are observed for different ranges of the Reynolds number. For two particles which interact while settling, a steady staggered structure, a periodic wake-action regime and an active drafting–kissing–tumbling scenario are realized at increasing Reynolds numbers. The nonlinear effects of particle–fluid, particle–wall and interparticle interactions are analysed, and the mechanisms controlling the simulated flows are shown to be lubrication, turning couples on long bodies, steady and unsteady wakes and wake interactions. The results are compared to experimental and theoretical results previously published.

1. Introduction

There are two different ways of looking at a two-phase system. One is the continuum approach that views solids and fluids as interpenetrating continua, each being governed by conservation laws, either postulated or derived by averaging, with transport terms representing the interaction of both phases (Ishii 1975; Drew 1983; Joseph & Lundgren 1990). The major difficulty is that these interaction terms are not known from the theory, and have to be otherwise specified to close the equations (Anderson & Jackson 1967). An alternative approach is to solve the equations for each phase exactly by numerical methods, moving the particles according to the equations of a rigid body with forces computed by direct simulation. This approach does not require assumptions and can be as exact as numerical methods will allow. The numerical solutions can be interrogated for the hydrodynamic forces that induce the micro-structural arrangements of particles which determine the macroscopic properties

of the flow. A drawback is that in fully nonlinear problems only a few particles can be handled at present, but the future is brighter.

Many-particle problems have been treated in the limit of zero Reynolds number by Brady & Bossis (1985) and Kim (1991). Problems of the motion of a few particles and bubbles at finite Reynolds number in three dimensions have been simulated using a front-tracking method by Unverdi & Tryggvason (1992). More recently, Kim, Elghobashi & Sirignano (1993) performed a three-dimensional numerical simulation of a steady flow past two fixed spheres at Reynolds numbers up to 150. A two-dimensional direct simulation of the motion of sedimenting circular and elliptic particles in a channel is given in Hu, Joseph & Crochet (1992*b*) using a finite element method, and a video of this simulation together with a short paper is given in Hu, Fortes & Joseph (1992*a*). The major difficulty concerns the nonlinear effects that arise when (*a*) the Reynolds number is large enough for inertia to be important, (*b*) the fluid is non-Newtonian and the flow is inherently nonlinear and (*c*) the particle is deformable. In this study, we will consider the case of rigid particles in Newtonian fluids only, so that inertia is the only form of nonlinearity besides the changing geometry.

There is an extensive literature using superposition of fundamental solutions (Stokeslets) in problems of the motion of interacting spheres in Stokes flow (Hocking 1964; Wacholder & Sather 1974). The extension to an assemblage of many particles has also been extensively explored (Happel & Brenner 1965; Feuillebois 1989; Hassonjee, Pfeffer & Ganatos 1992; Brady & Bossis 1985; Kim 1991).

Weak effects of inertia may be determined by perturbation of the Stokes solution for small Reynolds numbers. Particle–fluid interactions for slow flows have been discussed by Brenner (1966), Batchelor (1974) and Leal (1980). Leal (1980) has noted that the accumulative effect of weak inertia can produce large effects that are not in the linear theory. The anomalous effects predicted by these studies, such as the lateral migration of particles in a shear flow, agree qualitatively with experimental observations, some of them made in situations where the inertial effect is not at all weak. The success of first-order perturbation theories makes people wonder why in some cases strong nonlinearity does not seem to give additional features to the flow, and more importantly, whether this is true in other cases.

Explicit analytic solutions of fully nonlinear problems of fluid–particle motions are rare. Numerous codes have been developed to simulate nonlinearity by solving the full Navier–Stokes equations for situations such as flow around fixed bluff bodies. The problem of simulating the unsteady motion and interaction of particles raises an additional difficulty in that the boundaries of the computational domain are ever changing owing to the motion of the particles, and the coupling between solids and fluids is of a more complicated type. Hu *et al.* (1992*b*)'s adaptation of a Navier–Stokes solver, POLYFLOW, has been successful in dealing with the combination of full nonlinearity and fluid–solid coupling. At each time step, the previous flow field gives the force and torque on the particles, whose motion is then explicitly updated by Newton's law, giving rise to a new domain. After remeshing and mapping the old flow field onto the new mesh, the nonlinear Navier–Stokes equations are solved by a finite-element formulation, iteratively with the implicitly discretized Newton's equation for particle velocities, which are also part of the boundary conditions for the fluid flow. The purpose of this paper is to apply this code to various physically interesting flow situations involving strong inertial effects, interaction among particles and between particles and bounding walls. We do try to compare the results of our two-dimensional

simulation with experiments, understanding that the evolution of rules for such an unnatural comparison is also a topic that needs study.

We simulate the following flow situations in which particle–fluid, inter-particle and particle–wall interactions are fully manifested:

(i) The settling of a single circular particle through quiescent fluid between parallel walls. We study the initial value problem in which a particle is dropped from rest and we look at the drag, transients, bifurcation to time-dependent solutions, the trajectories of the particles and their position of equilibrium, and the influence of the ratio of channel width to particle diameter on the flow.

(ii) The settling of an elliptic particle in the same channel. We will study the lateral position of equilibrium as well as the preferred orientation of the particle.

(iii) Sedimentation of two particles in a channel. We will give special attention to the pattern of interactions among the particles.

Because these problems involve many complicated effects and comparable studies, either numerical or experimental, are rare, we feel it necessary to use relatively simple test problems to further confirm the validity of our simulation. Therefore, we have computed, as test cases, the steady flow around a fixed circular cylinder and the unsteady flow caused by the abrupt start-up of a slender elliptic cylinder at incidence.

In the following sections, we will first discuss the test problems, which do seem to validate our code. Then, numerical results will be presented on each problem listed above and discussed in association with available experimental observations as well as previous theoretical results.

2. Test problems

The steady flow around a circular cylinder fits our requirement here because it has been thoroughly studied and documented. To test the code's ability to handle transient Navier–Stokes problems, we choose the problem of impulsive acceleration of an elliptic cylinder in a quiescent fluid, as it has also been systematically explored by many researchers, e.g. Honji (1972) and Taneda (1977) experimentally, and Lugt & Haussling (1974), Patel (1981) and Park, Park & Hyun (1989) numerically. Besides, this problem reveals the hydrodynamics associated with the formation and shedding of vortices behind a slender body. It has a practical relevance and is by itself interesting as reflected by recent studies (Shintani, Umemura & Takano 1983; Ota & Nishiyama 1984).

A circular cylinder (diameter d) is fixed at the centre of a channel of width $20d$. Computation is carried out for $Re = 40$. The streamlines and isovorticity lines are shown in figure 1. These are seen to be in good agreement with the classic results of Apelt (1961). In figure 2, the pressure distribution on the surface of the cylinder is compared to the numerical calculations of Apelt (1961) and Fornberg (1980), and to some experimental data that Thom (1933) measured at slightly different Reynolds numbers. The pressure coefficient we computed agrees well with the data of Apelt (1961) and Thom (1933), but is considerably smaller than Fornberg's C_p, especially around $\theta = 90°$ where C_p has a minimum. This is probably because Fornberg used an extremely large domain to avoid the influence of channel blockage. If we estimate the pressure as varying with the square of the local velocity (Bernoulli's equation), blockage will reduce C_p greatly. This has been verified by our numerical experiments using channels of different width.

The second numerical example involves a slender ellipse of aspect ratio 10.03 which is placed in the middle of a two-dimensional channel of width $4d$, d being the length

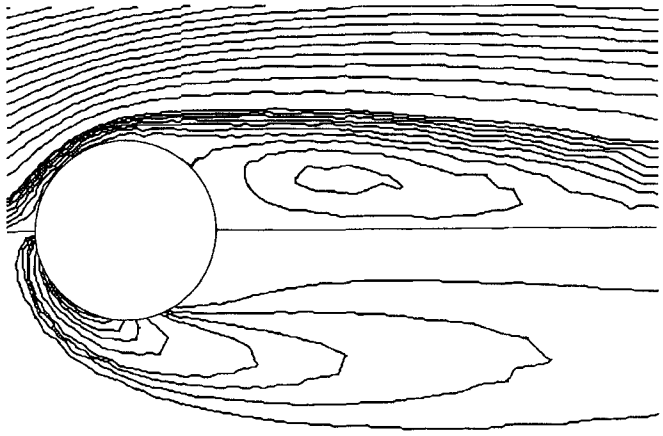

FIGURE 1. The streamlines and isovorticity lines of a steady flow around a fixed circular cylinder at $Re = 40$. The flow is from left to right.

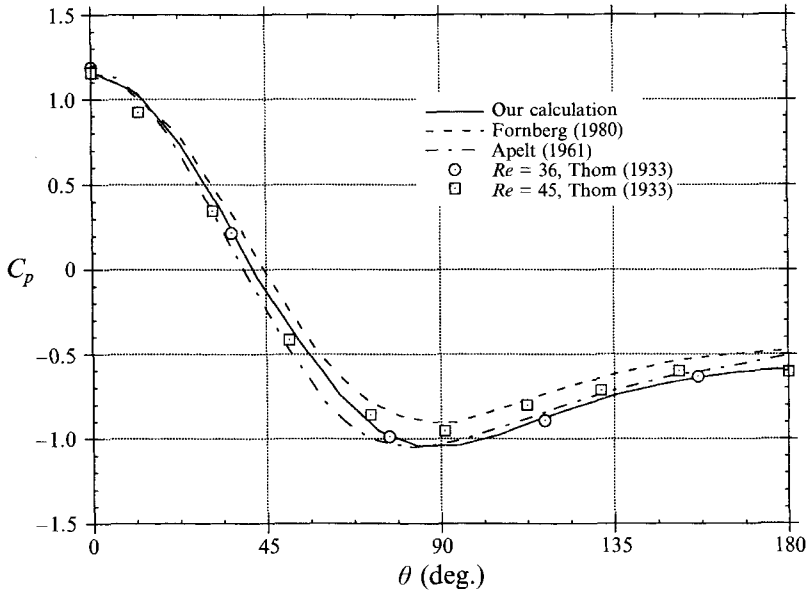

FIGURE 2. Pressure distribution on the surface of the cylinder. Apelt (1961), Fornberg (1980) and our calculation are at $Re = 40$.

of the major axis. The ellipse makes an angle of 45° with the walls of the channel. At $t = 0$, the ellipse instantly gains a constant velocity U in the direction of the channel wall that corresponds to $Re = Ud/\nu = 200$. The geometry of the ellipse, the angle of attack and Re are the same as in Lugt & Haussling (1974) to facilitate comparison. The initial condition is $(u, v) = (U, 0)$ everywhere except on the surface of the body, where zero velocity is implemented for all time. The channel walls are specified as undisturbed streamlines. The inlet of the domain is $10d$ ahead of the body, where uniform velocity U is applied, while the outlet is $15d$ downstream of the body, where normal derivatives of velocity are set to zero. This outer boundary is different than the elliptic coordinate boundary Lugt & Haussling (1974) adopted. They imposed the potential flow solution around the ellipse on the outer boundary which is determined by an elliptic coordinate.

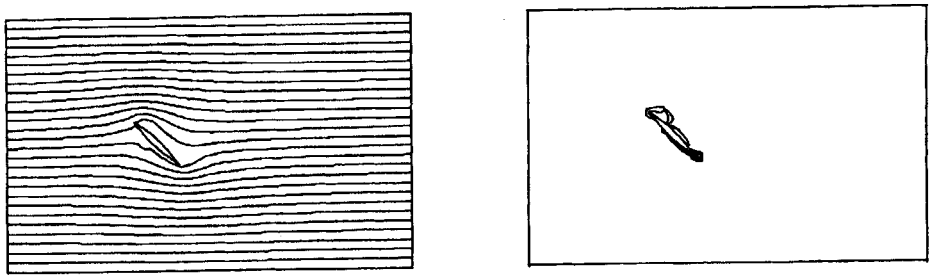

(*a*) $t^* = 0.2$

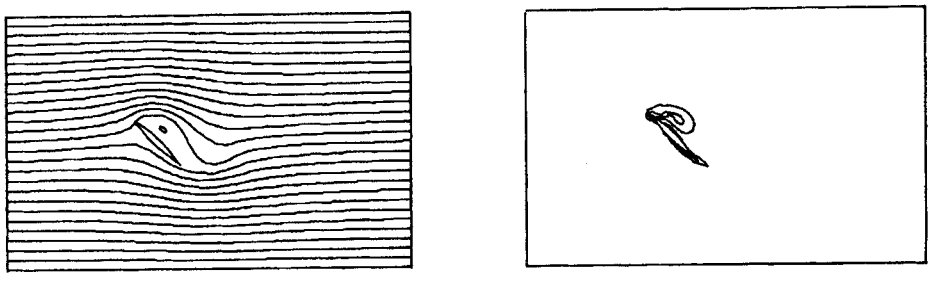

(*b*) $t^* = 0.8$

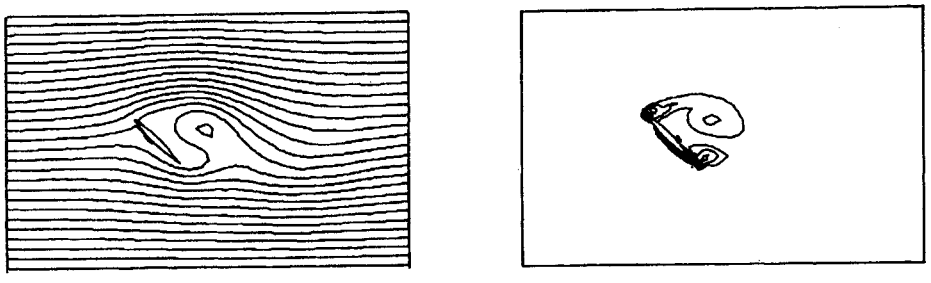

(*c*) $t^* = 2.6$

FIGURE 3. Streamlines and isovorticity lines for the early stages of flow field development. Dimensionless time $t^* = Ut/d$.

Early stages of the developing flow field are shown in figure 3(*a–c*). Because we used a coarse mesh and the remeshing package does not perform as well on surfaces of large curvature, the streamline near the front surface is not smooth for some cases. Apart from that, the evolution of the flow is much the same as the numerical predictions of Lugt & Haussling (1974) and Patel (1981), Honji (1972)'s visualization verifies those pictures. We note that our timescale is different than that in Lugt & Haussling, but in terms of the dimensionless time $t^* = Ut/d$, the two results agree perfectly.

After the initial transient, a periodic flow is achieved with vortices shedding alternately from both ends of the slender body. A complete cycle is shown in figure 4(*a–e*). The general pattern of flow is again in agreement with previous numerical results (Lugt & Haussling 1974; Park *et al.* 1989). We have noticed, however, that our wake is narrower and longer than Lugt & Haussling's for the same parameters. The reason for this difference is probably the strong wall confinement in our problem. The oscillatory pattern and mean values of the drag, lift and moment on the body are all

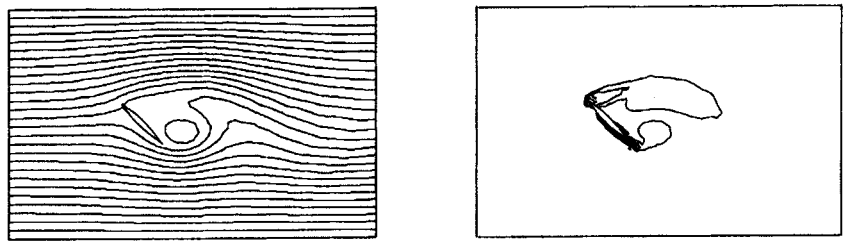

(*a*) $t^* = 3.6$

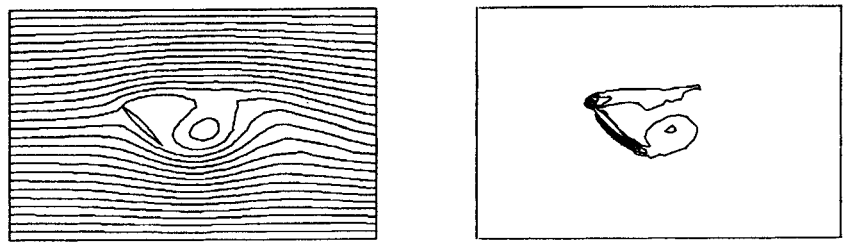

(*b*) $t^* = 4.6$

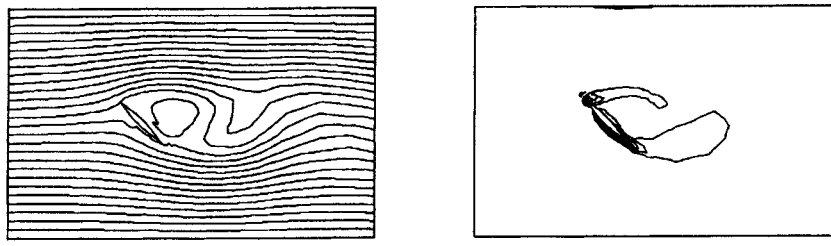

(*c*) $t^* = 5.6$

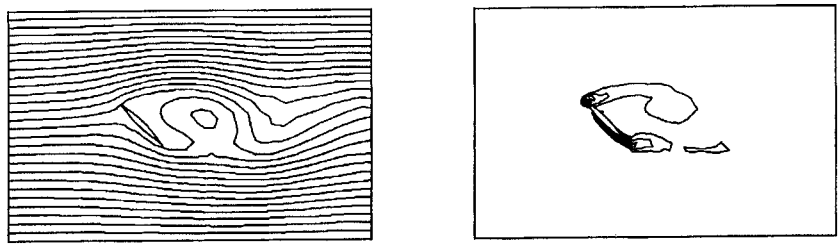

(*d*) $t^* = 6.6$

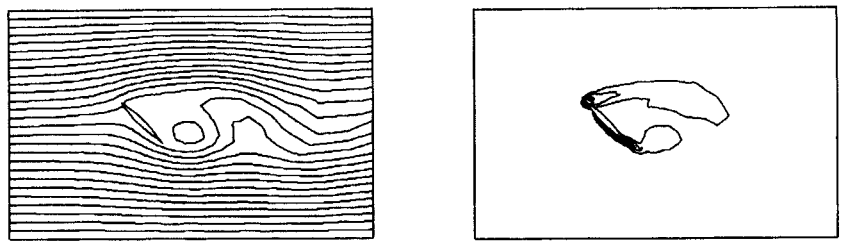

(*e*) $t^* = 7.6$

FIGURE 4. Streamlines and isovorticity lines for a cycle of vortex shedding behind the body.

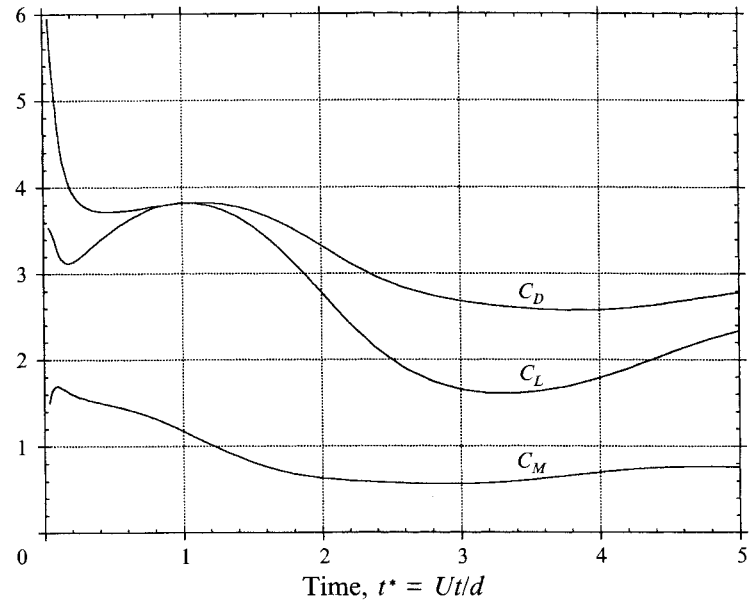

FIGURE 5. The drag, lift and moment coefficients on the elliptic cylinder after its abrupt start-up.

very close to those of Lugt & Haussling (1974) (figure 5). Actually, the Strouhal numbers for the first two cycles are 0.23 and 0.25 in our case, as compared to 0.23 and 0.26 in Lugt & Haussling. But the amplitude of oscillation is smaller here, and it decreases more rapidly at the beginning.

In conclusion, comparison of the simulations of test problems using our code and previously published results indicates that our solver works with acceptable accuracy, and we can apply it to more complex problems.

3. Settling of a circular particle between parallel walls

A circular particle of diameter d is released from different lateral positions, with zero initial velocity, in a channel of width L. The x-axis is vertically down on the left wall, and the y-axis horizontal to the right. The initial position of the centre of the particle is therefore $(0, y_0)$. The particle is heavier than the fluid and starts to settle under gravity. In the absence of inertia, the particle would settle straight down with no lateral motion (Happel & Brenner 1965). This is no longer the case when inertia becomes important. By varying the density of the particle, we are able to control the mean terminal velocity and to access Reynolds numbers (based on the particle diameter) corresponding to different regimes of sedimentation. Five intervals of Re can be demarcated in terms of the mean position of equilibrium, the approach to equilibrium and the presence or absence of oscillation around the equilibrium. For each computation, numerical tests were carried out for an extended time period to ensure that the results obtained represent the long-time behaviour correctly.

We have used three channels of different width ($L = 1.5d$, $4d$ and $8d$) in our computation. Major features of the sedimentation are the same in all channels, and the behaviour of the particle can be classified into five regimes which occur at different Reynolds number intervals depending on the channel width. We will first establish the flow regimes for one channel width $L = 4d$. Results for the other two channels will then be discussed as associated with wall effects.

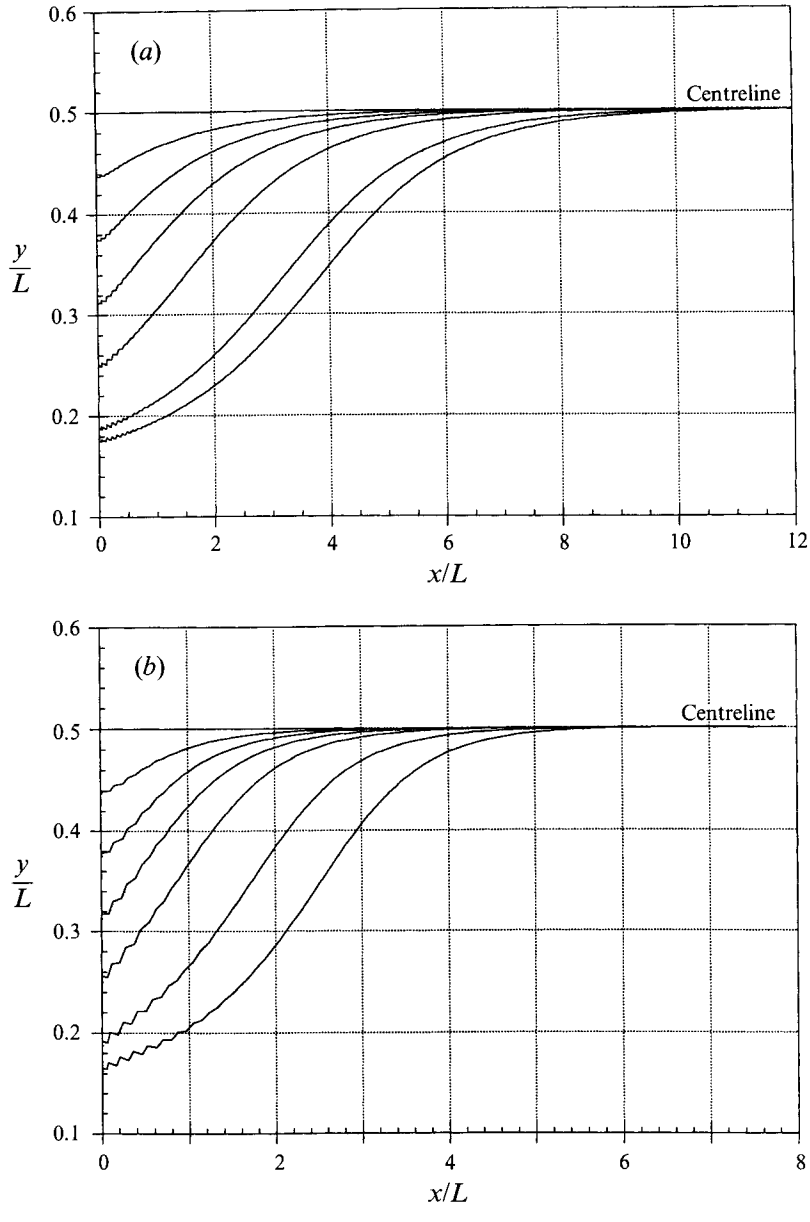

FIGURE 6. Regime A: settling trajectories for particles released from different initial positions. (*a*) $Re = 0.522$, (*b*) $Re = 1.03$. Channel width $L = 4d$, d being the diameter of the circular particle. The centre of the channel is a global attractor.

3.1. *Flow regimes*

Regime A: Steady equilibrium with monotonic approach ($0.1 < Re < 2$)

The particle drifts monotonically to a steady equilibrium on the centreline of the channel independent of the initial position of the particle. When starting from an initial position off the centre, the particle will rotate until it reaches the centreline where the rotation stops. The sense of rotation is always such that the particle seems to roll up the closer wall. The trajectories for $Re = 0.522$ and 1.03 are shown in figure 6(*a*, *b*). The small wiggles at the beginning of the sedimentation are due to numerical errors

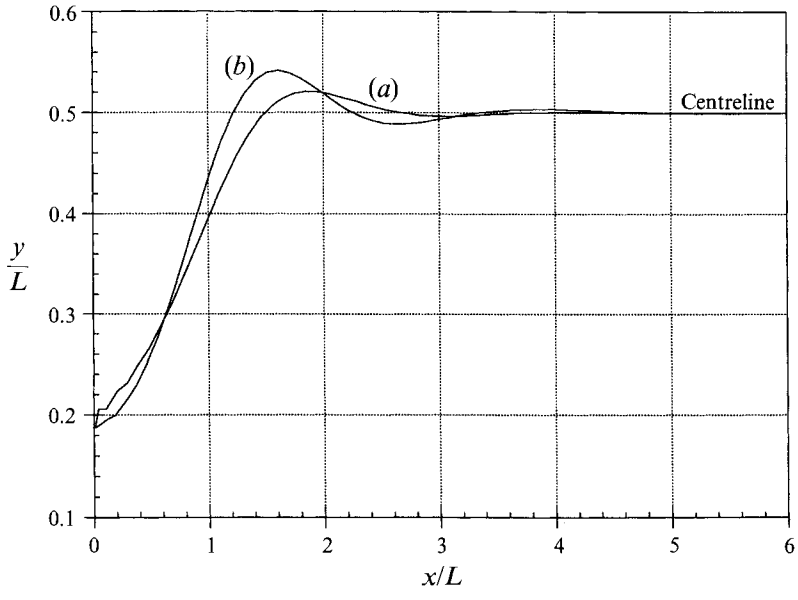

FIGURE 7. Regime B: settling trajectories of particles at (*a*) $Re = 3.23$, (*b*) $Re = 8.33$.

associated with explicit updating of particle positions, and are apparent only when the settling velocity is small. The range of low Reynolds number $0.1 < Re < 2$ is arbitrary. Inertia will eventually have its way at any Reynolds number, no matter how small.

Regime B: Steady equilibrium with a transient overshoot ($3 < Re < Re_{crit}$)

In this regime, the centre of the channel is still an equilibrium position, but the approach to it is not monotonic. There is an initial overshoot followed by a damped oscillation. The angular position of the particle also has an overshoot, but the rotation will finally vanish after the particle stabilizes on the centreline. Shown in figure 7 are the trajectories of particles released near the wall at two Reynolds numbers.

Regime C: Weak oscillatory motion ($Re_{crit} < Re < 60$)

When the Reynolds number exceeds a critical value, the steady equilibrium position at the centre of the channel becomes unstable, and the long-term behaviour of the particle is a weak oscillation around an equilibrium position slightly off-centre. This off-centre distance becomes larger as Re increases (figure 8). In the $4d$ channel, the critical Reynolds number is probably in the twenties. The upper bound of this regime is set by considering the advent of the strong oscillatory motion caused by vortex shedding.

Regime D: Strong oscillatory motion ($60 < Re < 300$)

Some typical trajectories are compared in figure 9(*a*). As compared to regime C, the particle oscillates with much larger amplitude around a mean equilibrium position that is further away from the centreline. The oscillation is not monochromatic, but it may be periodic with a modulation in the amplitude. Once the particle is off the centre, the wall effect imposes a unidirectional rotation on the particle, as is shown in figure 9(*b*). Contrary to regimes A and B, the sense of rotation here is such that the particle seems to roll down the nearby wall. The oscillations in rotation and trajectory are locked and have the same frequency. The upper and lower bounds of this interval are set somewhat arbitrarily.

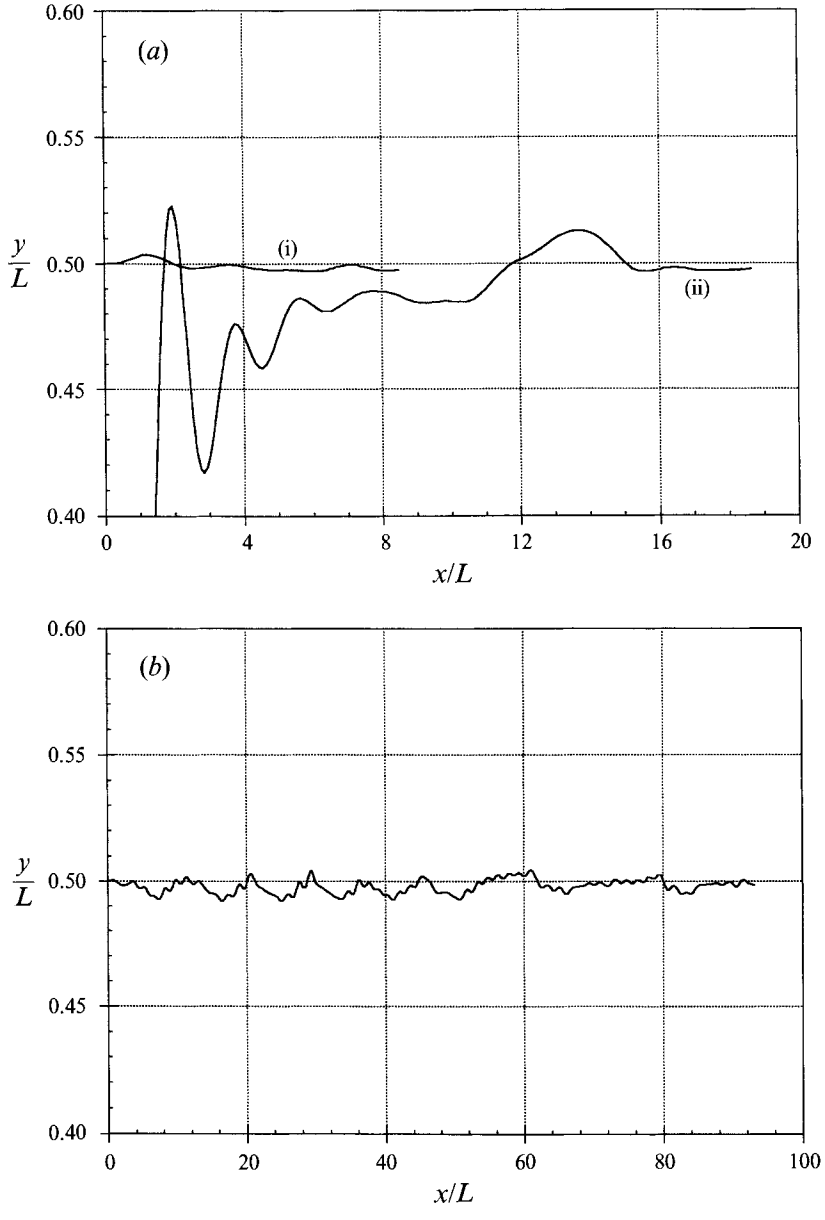

FIGURE 8. Regime C: settling trajectories at different Reynolds numbers. (*a*) $Re = 27.6$, particle released from (i) the centre, $y_0/L = 0.5$, (ii) an initial position close to one wall, $y_0/L = 0.13$; (*b*) $Re = 50.6$, particle released from the centre.

Regime E: Irregular oscillatory motion ($Re > 300$)

If Re is further increased in the last regime, we expect the periodic behaviour to become unstable and break down into less regular patterns. Indeed, this seems to be the case at $Re = 490$ (figure 10). The long-term dynamics of the flow may be chaotic, but we cannot distinguish numerical noise from chaos in that extreme.

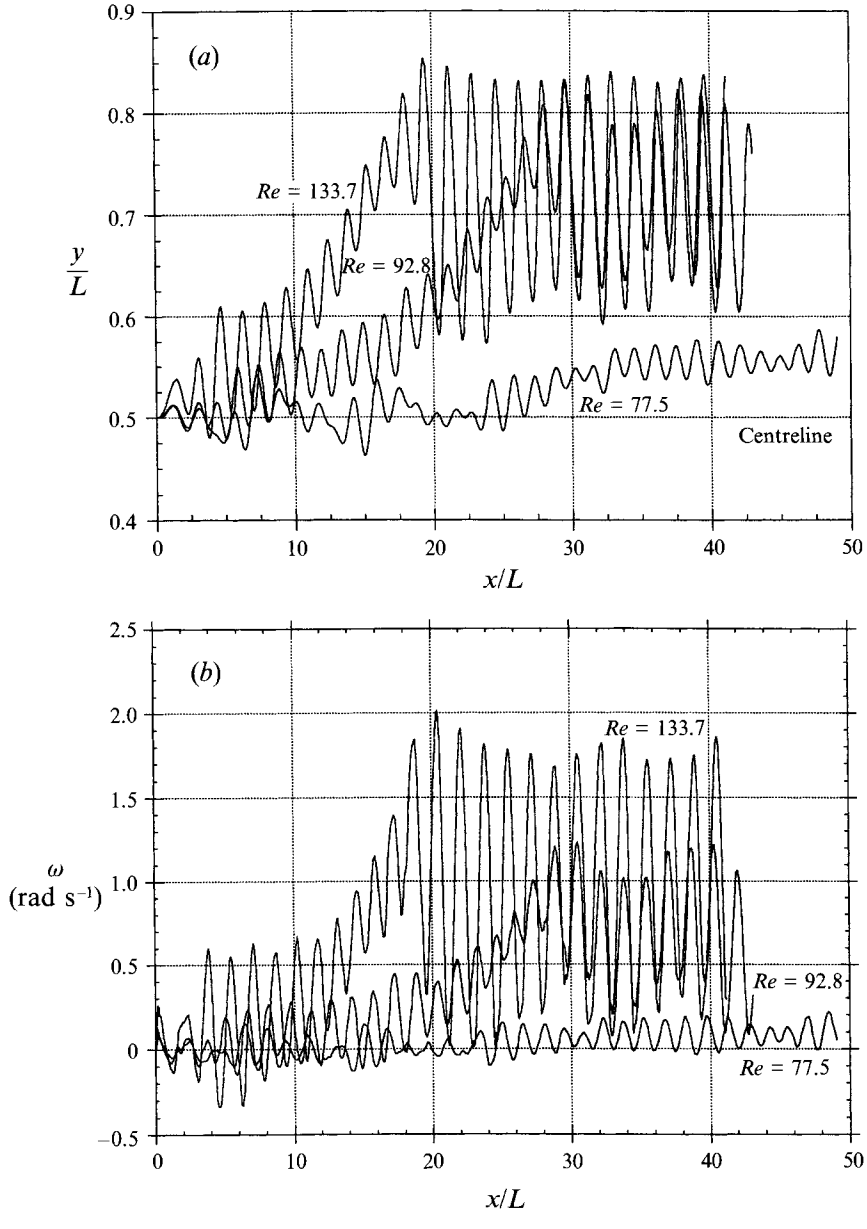

FIGURE 9. Regime D: sedimentation of particles at relatively high Reynolds numbers. (*a*) Settling trajectories, (*b*) angular velocities.

3.2. *Analysis of the flow regimes*

A natural way of understanding the above regimes is by examining the local flow around the particle at different Reynolds numbers. Indeed, looking through the five regimes, it is immediately clear that they are closely related to the different phases of the wake structure behind a fixed circular cylinder in a uniform flow. Our problem is different from the fixed cylinder problem because of wall effects and the unsteady trajectory of the cylinders. But it is still illuminating to compare our regimes with well-established experimental observations of uniform flow around circular cylinders (Gerrard 1978; Morkovin 1964).

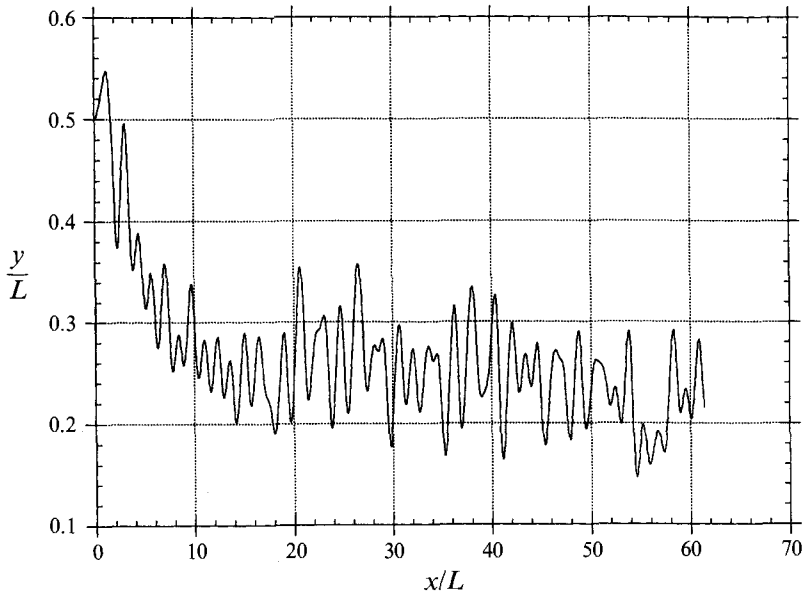

FIGURE 10. Regime E: settling trajectory of a particle released from the centre at $Re = 490$.

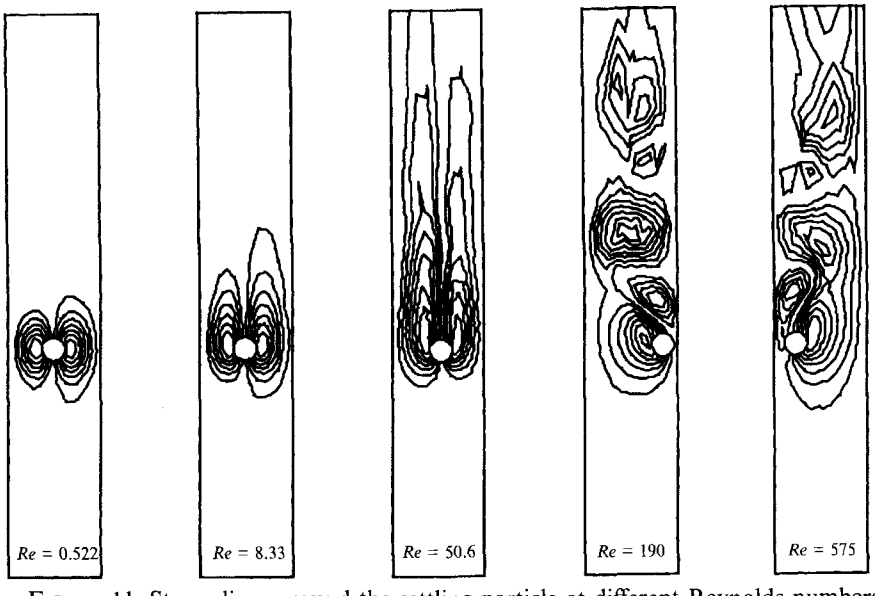

FIGURE 11. Streamlines around the settling particle at different Reynolds numbers.

At Re below 3, the inertia of a fluid flowing around a fixed cylinder is already considerable, but still not strong enough to produce a circulation zone (see figure 11 for the streamlines at different Re). This corresponds to our regime of monotonic approach to a steady equilibrium. At about $Re = 3 \sim 5$, steady and symmetric standing eddies emerge on the rear side of the cylinder, and remain till Re equals about 30, when they become unsteady. This corresponds to our regime B in which particles approach the centreline with overshoot. It is not certain whether the separated wake is directly responsible for the overshoot, or the inertia is just strong enough at that stage. Then steady standing vortices give way to a wavy but still attached wake, which becomes more unsteady until periodic vortex shedding starts at about $Re = 60$ to form

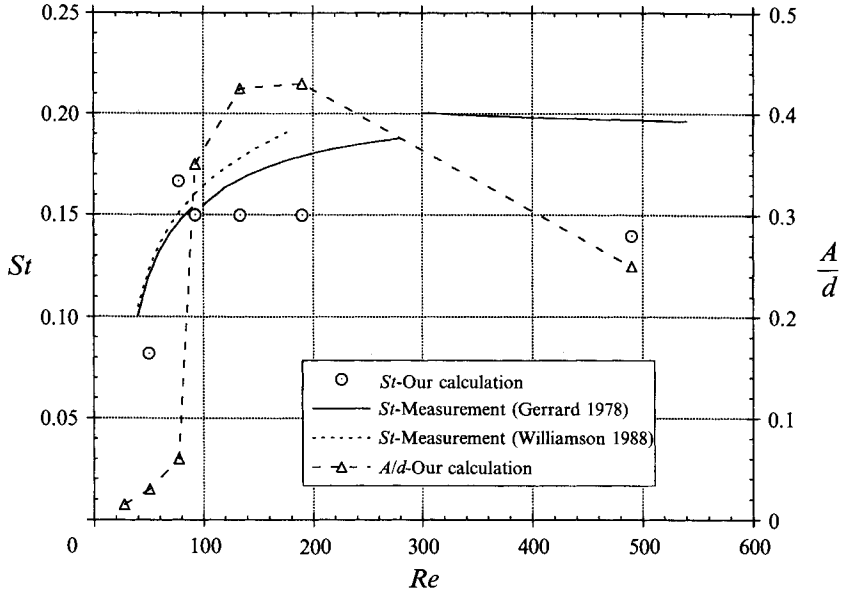

FIGURE 12. Amplitude and frequency of the oscillation in regimes C, D and E. The calculated frequency, represented by the Strouhal number $St = fd/U$, is compared to the measurements of Gerrard (1978) and Williamson (1988).

the Kármán vortex sheet. In our simulation, this stage corresponds to the regime of weak oscillatory motion. The critical Reynolds number for the onset of unsteadiness is smaller than its counterpart for a fixed cylinder in an unbounded fluid. This is because of the confinement of the walls, and the effect will be further addressed in §3.3. The Kármán vortex street, which prevails at about $60 < Re < 300$, is responsible for the persistent oscillation in regime D.

Another important feature of regimes C and D, the drift off the centreline, is obviously related to the wall effect and cannot be explained from the wake structure alone. We believe that the mechanism is a potentially destabilizing lift force related to particle rotation. At small Reynolds numbers, a particle released near the wall will rotate as if it is rolling up the wall. This is well known in the literature and is probably due to wall blockage. This rotation gives rise to a Magnus type of lift that tends to move the particle away from the wall. In the high-Re regimes, the sense of rotation is reversed and the lift force tends to move the particle off the centreline. If this lift is strong enough to dominate the wall repulsion, and the unsteadiness in the wake causes large enough sidewise disturbance, the equilibrium at the centreline will become unstable. The synchronization of the onsets of the drift and the persistent rotation in figure 9(*a*, *b*) appears to support the above explanation. This mechanism will be further discussed in §4.1 where it is related to sedimentation of an elliptic particle at high Reynolds numbers.

Finally, the irregular oscillation regime in our simulation is readily identified with the instability in the wake of a cylinder that happens around $Re = 300$ as the first indication of transition to a more chaotic flow field that eventually evolves into turbulence (Morkovin 1964).

If we look more carefully at the numerical results, further evidence of the wake action can be discerned. For example, the amplitude of oscillation in regime D is determined by the strength of vortex shedding which increases with Re, causing a wider

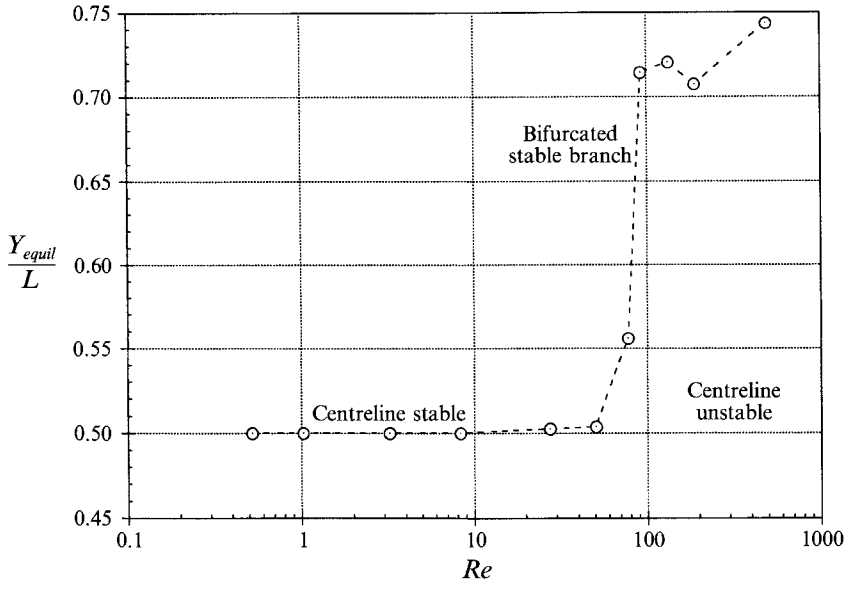

FIGURE 13. Mean equilibrium position as a bifurcation variable.

wake until the Kármán vortex street becomes unstable and the loss of periodicity in vortex shedding starts to diminish the sidewise actions on the cylinder. This is clearly reflected in the simulation (figure 12). The frequency of oscillation, however, shows quite different behaviour than that observed for a uniform flow around a fixed cylinder in an unbounded domain. This is easily understood by realizing that in addition to the purely periodic lift caused by vortex shedding, a wall effect must also be considered. This wall effect depends on the position of the particle in the channel, which changes continuously due to vortex shedding.

We can also look at the evolution of particle behaviour in terms of instability and bifurcation. In the first two regimes, the centre of the channel is a globally stable equilibrium position, and the motion of the particles is stable after the initial transient. As Re increases, this steady motion becomes unstable and is replaced by an oscillatory motion. At the same time, the mean equilibrium position moves away from the centreline, giving rise to a diagram (figure 13) that looks like a pitchfork bifurcation. The oscillatory solution loses its stability later and evolves into a more complicated motion. A prudent researcher might question the fact that the oscillation in regimes C and D is not perfectly periodic, and is subject to some irregularity. A plausible argument is that factors such as wall effect are inherently non-periodic, and will undermine the periodicity so as to induce apparent irregularity. This seems to be the case in a recent numerical simulation of a particle–spring system in a uniform flow (Nomura & Hughes 1992, figures 10 and 13). It is also possible, however, that the numerical methods in both studies are simply not accurate enough. At this point, we are not certain whether this aspect of our simulation is a correct description of the motion or is a defect of our numerical code.

3.3. *Wall effects*

The major features of the sedimentation discussed above also occur in the other two channels with different width: $L = 1.5d$ and $8d$, although at different Reynolds number intervals. The wall effects are examined in various regimes here.

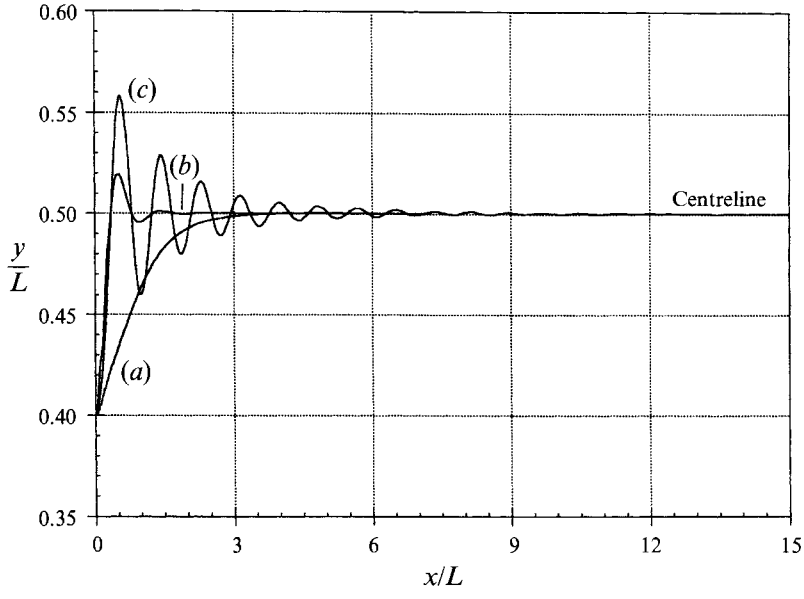

FIGURE 14. Trajectories of particles settling in the steady equilibrium regimes in the narrow channel ($L = 1.5d$) at various terminal Reynolds numbers: (*a*) $Re = 0.65$, (*b*) $Re = 3.23$, (*c*) $Re = 6.28$.

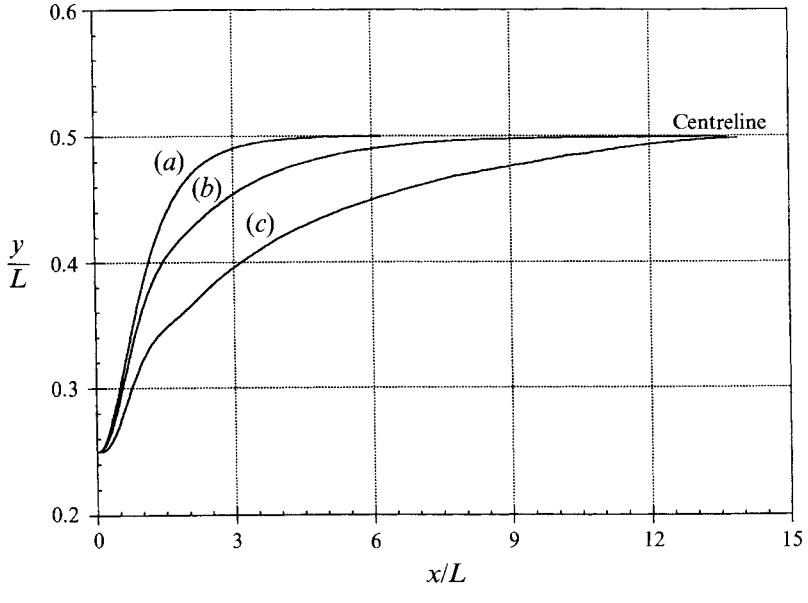

FIGURE 15. Trajectories of particles settling in the steady equilibrium regimes in the wide channel ($L = 8d$) at various terminal Reynolds numbers: (*a*) $Re = 1.96$, (*b*) $Re = 5.27$, (*c*) $Re = 12.0$.

(i) The steady equilibrium regimes, either with or without overshoot, are dominated by the wall repulsion, and so the Reynolds-number intervals are shifted up in a wider channel. This is made clear by comparing figures 14 and 15 with figures 6 and 7. Actually, in the $8d$ channel the wall effect is so much weaker that a smooth overshoot is not observed until the steady solution loses stability.

(ii) The onset of instability of steady sedimentation is decided by the flow field around the particle, which is also affected by the walls. This happens very early in the

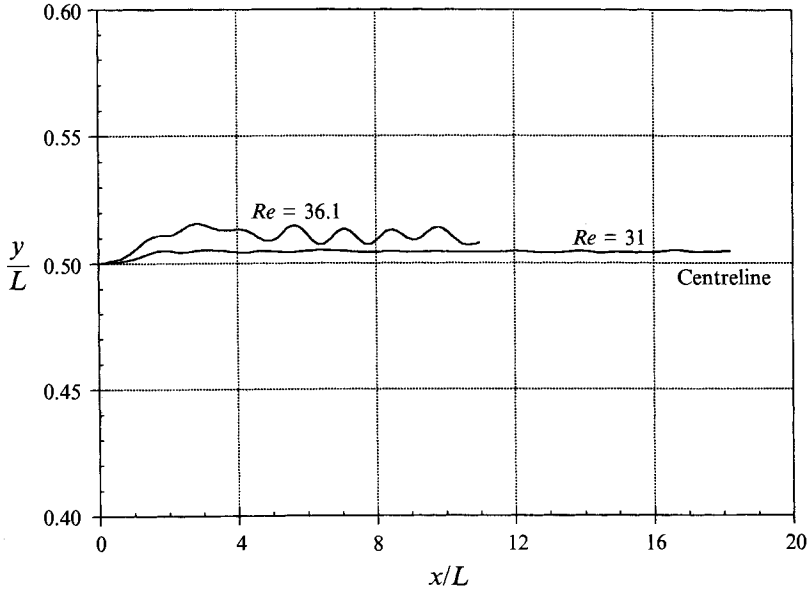

FIGURE 16. Weak oscillatory motion in an $8d$ channel shortly after the steady solution bifurcated.

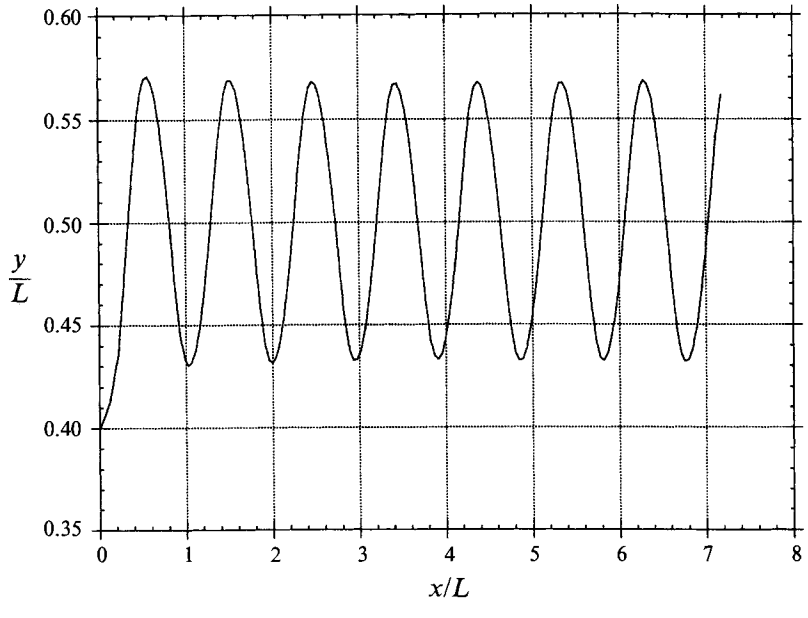

FIGURE 17. Periodic oscillation of a particle settling in the narrow channel at $Re = 10.7$ based on the mean velocity.

narrow channel ($L = 1.5d$) because of the strong blockage effect; the critical Reynolds number for bifurcation is below the value $Re = 10.7$ for which a well-developed periodic solution is evidently stable (figure 17). In the wide channel ($L = 8d$), the instability probably first becomes appreciable around $Re = 30$ (figure 16). We have not carried out a detailed search for points of bifurcation and we cannot assert that the critical Reynolds number increases monotonically with channel width.

(iii) Perfect periodic solutions are obtained in the narrow channel, and the mean

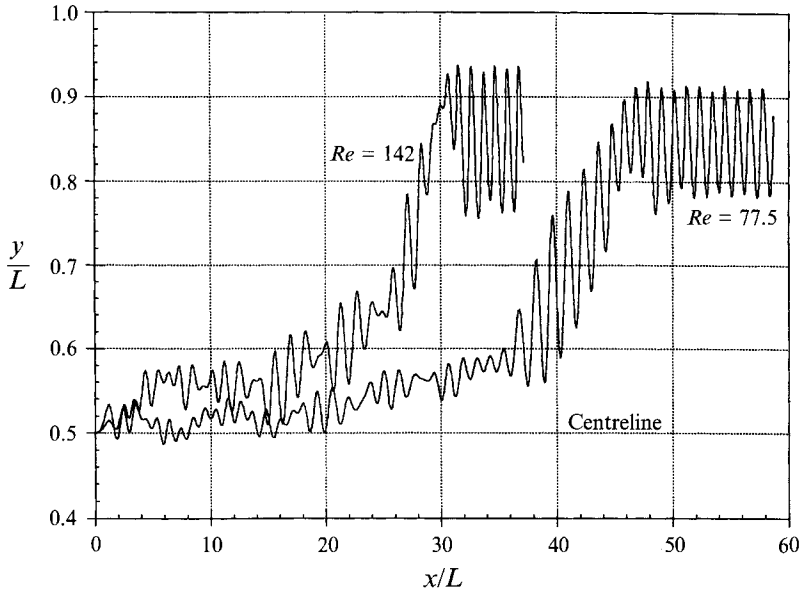

FIGURE 18. Strong oscillatory motion of particles settling in the wide channel at two Reynolds numbers.

position of the particle never drifts away from the centreline (figure 17). This is a direct result of the strong wall repulsion. Streamlines show that vortex shedding exists at Reynolds number as low as 10.7. In the wide channel ($L = 8d$), oscillatory motion similar to figure 9 is obtained after a long transient (figure 18). Again, we do not understand the origin of the irregular variation of the amplitude. In a wider channel, the particle's mean position tends to be closer to the wall.

Owing to the high cost, the regime of irregular oscillatory motion at higher Reynolds number has not been examined in the wide and narrow channels.

3.4. *Drag coefficient*

From our simulation, a drag coefficient on the particle can be calculated using the mean terminal velocity U:

$$C_d = \frac{\pi}{2}\left(\frac{\rho_s}{\rho_f} - 1\right)\frac{gd}{U^2},$$

where ρ_s, ρ_f are the densities of the particle and the fluid; g is the gravitational acceleration.

The results in all three channels are compared in figure 19, along with data from other sources. The 'standard drag' is an empirical correlation of experimental data on a fixed cylinder in an unbounded domain (Sucker & Brauer 1975). Fornberg's (1980) result is from a numerical computation for steady flow around a cylinder in a very large domain. Our numerical results shows that wall confinement generally increases the drag, up to 50 times in the narrow channel. This effect decreases with Re. In the wide channel, the drag comes very close to the standard drag at $Re \approx 30$. Fornberg's drag coefficient is consistently smaller than the experimental results. Another interesting point is that after the steady equilibrium bifurcates and the particle drifts off the centreline, there is a sudden increase in the time-averaged drag with Re. This is evidently related to the fact that the particle is close to a wall.

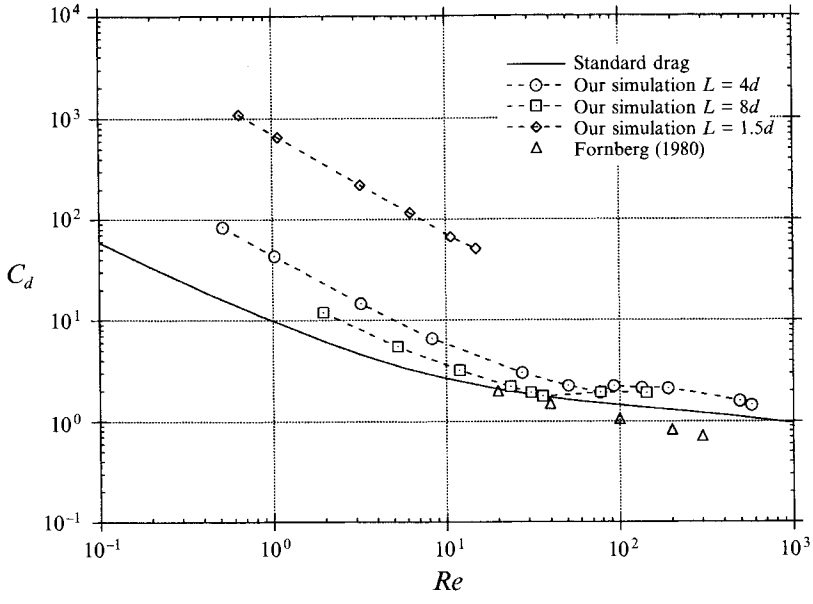

FIGURE 19. Drag coefficients of a particle settling in various channels as compared to the standard drag (Sucker & Brauer 1975) and the numerical result of Fornberg (1980).

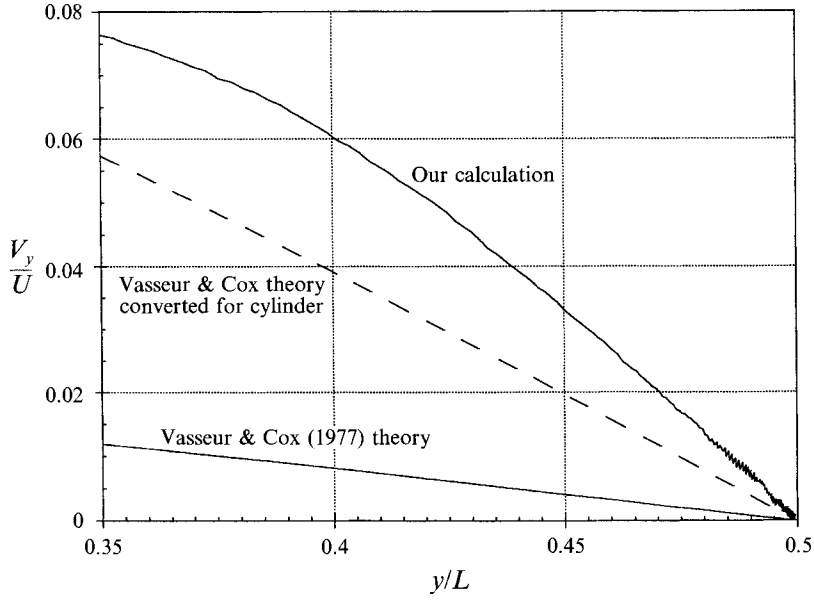

FIGURE 20. Comparison of migration velocity between our calculation ($Re = 0.522$) and the perturbation theory of Vasseur & Cox (1977). U is the terminal velocity of the particle in an infinite fluid. The centreline is at $y = 0.5L$. A factor of 4.8 is applied to Re to convert their three-dimensional theory for comparison to our two-dimensional calculation as explained in the text.

3.5. *Comparison with other results*

As mentioned in the introduction of this paper, we should try to relate two-dimensional numerical simulations to three-dimensional flow situations. A systematic comparison with relevant experiments and theories is therefore necessary. Because almost all of the

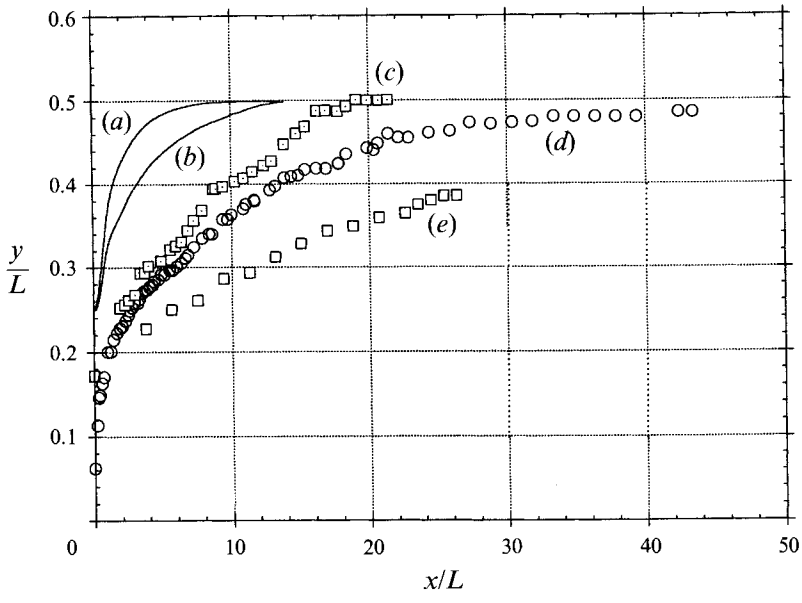

FIGURE 21. Comparison of our simulation for an $8d$ channel ((*a*) $Re = 5.27$, (*b*) $Re = 12$) with experimental and theoretical data on sedimentation of a single sphere at small Reynolds number: (*c*) our experiment at $Re = 74.5$, (*d*) our experiment at $Re = 7.85$, (*e*) Vasseur & Cox (1977) at $L = 38.6d$, $Re = 0.093$.

experiments have used spherical particles, we at least have to convert the Reynolds number to ensure meaningful comparison, since circular cylinders have almost exactly the same wake structure as spheres, only at a much lower Reynolds number. Let us use the separation Re as a rough criterion. For spheres, circulation zones first appear at about $Re = 24$ while for cylinders $Re = 5$ (Van Dyke 1982). Thus a ratio of 4.8 will be applied hereafter whenever a conversion is needed.

On the lower end of the Re spectrum, we have to mention the perturbation analysis of Vasseur & Cox (1977). Their theory, like all other theories of its kind, is unable to follow the actual motion of the particle. Instead, they can only calculate the lateral force experienced by a particle if it were settling vertically in a channel at constant speed. Then they defined a 'migration velocity' by the Stokes drag:

$$v_l' = F_l'/(6\pi a\mu),$$

where a is the radius of the sphere and F_l' is the lift force. Within the confines of their approximations, they have shown that no matter where the particle is, the lift force acts like a resultant of the repulsion from both walls and tends to move it to the centreline. This is in agreement with our simulation in the low-Re regime. If we assume that the lateral migration is of constant speed, then their v_l' can be compared to our migration velocity after applying the aforementioned ratio of 4.8 (figure 20). The numerical discrepancy should not be surprising, since their theory is valid for vanishing Re only and includes other assumptions about the particle's motion.

To support their theory, Vasseur & Cox also did experiments on the sedimentation of a small sphere in a vertical duct of a rectangular cross-section. The aspect ratio was 6:1 so that the effect of the two widely spaced walls may have been negligible. They observed migration away from the wall to the centreline between the two closely spaced walls at $Re = 0.093$. Tachibana (1973), working with spheres settling in a vertical round pipe, observed a similar phenomenon at $Re = 7.3$. In our laboratory, we have

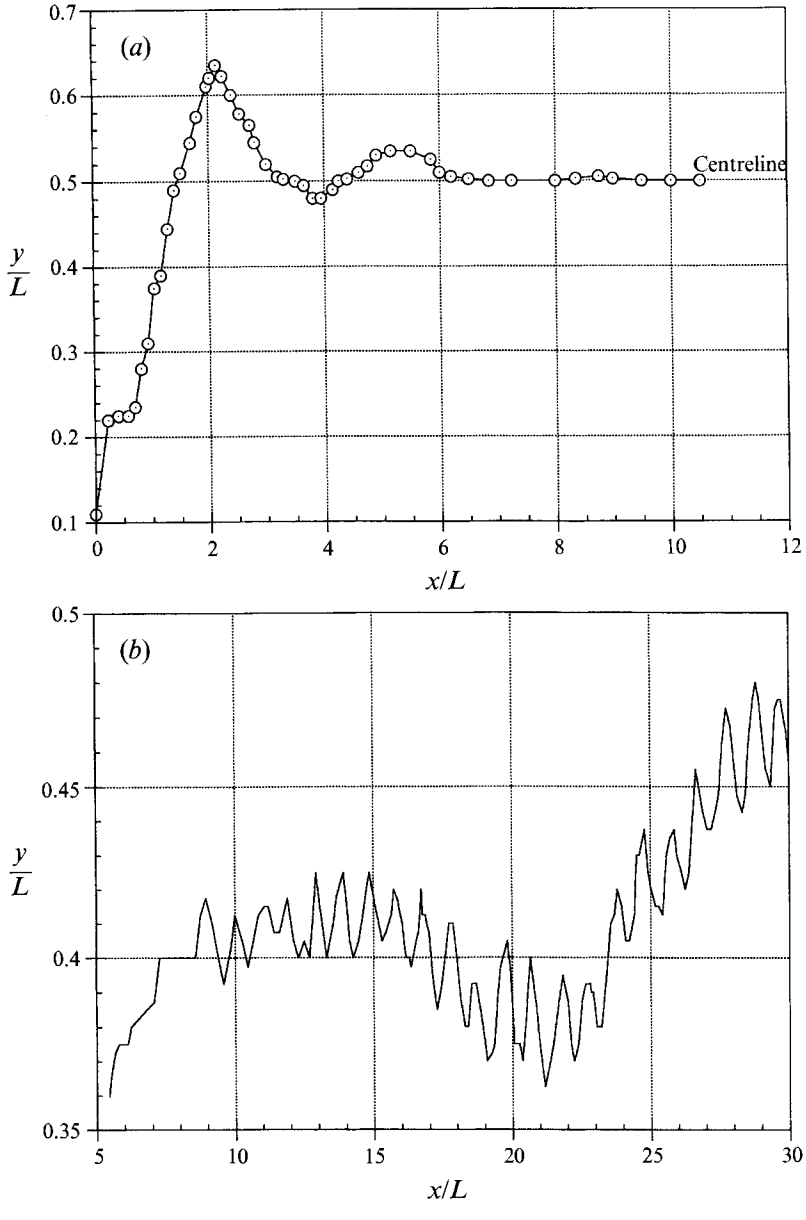

FIGURE 22. (*a*) Settling of a sphere in 35% glycerin in water in a narrow ($L = 4d$) 'two-dimensional' channel. Particle diameter $d = 0.25$ in., $Re = 256.9$. (*b*) Settling of a sphere in 30% glycerin in water in a wide ($L = 8d$) 'two-dimensional' channel. Particle diameter $d = 0.25$ in., $Re = 348.8$.

used two 'two-dimensional' columns with very high aspect ratio such that the particles are confined to virtually plane motion (Fortes, Joseph & Lundgren 1987; Volpicelli, Massimilla & Zenz 1966). The width of the channels used is 1 in. for the narrow channel and 2 in. for the wide channel. The fluid used in the channels is an aqueous solution of glycerin, whose density and viscosity can be changed with the concentration of glycerin. Again, spherical particles (diameter $d = 0.25$ in.) migrate away from the wall to the centre of the 'two-dimensional' channel at relatively small Reynolds numbers. A comparison of these experimental data with our simulation is shown in

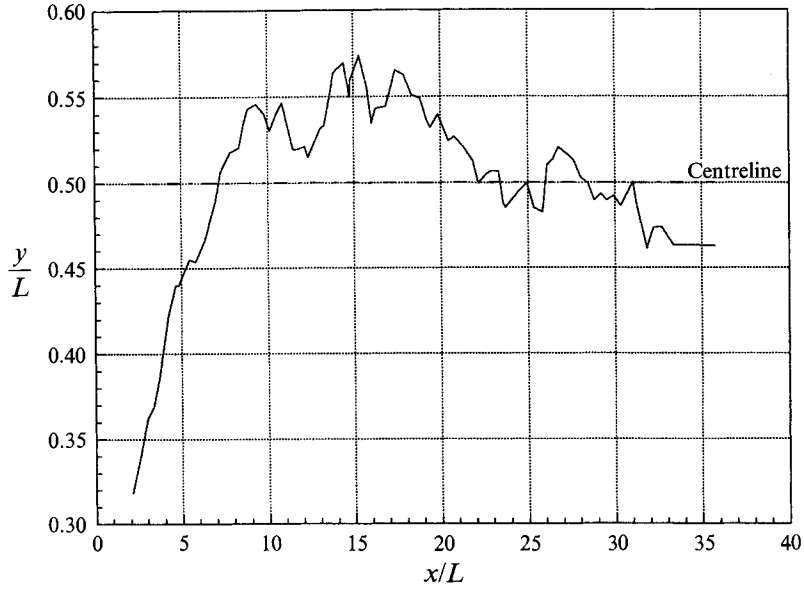

FIGURE 23. Settling of a circular particle in 20% glycerin in water in a wide ($L = 8d$) 'two-dimensional' channel. The particle is a short circular cylinder with its axis kept horizontal in the 'two-dimensional' channel. Particle diameter $d = 0.25$ in., length $= 0.25$ in., $Re = 443.6$.

figure 21. Obviously, the overall migration is correctly simulated, although quantitative discrepancies exist for understandable reasons. We see dynamic similarity between two-dimensional simulations and experiments in three dimensions using a 'two-dimensional' bed, but at different Reynolds numbers much greater than our 4.8 factor of conversion, and with no systematic difference. Evidently two-dimensional simulation has a restricted application to three-dimensional motions in a 'two-dimensional' bed.

Denson, Christiansen & Salt (1966) observed the under-damped oscillatory motion predicted by our simulation in regime B for a wide range of Reynolds number ($16 \sim 120$). Repetti & Leonard (1966) reported similar behaviour. Although their flow situations are different (buoyant particle migration in a pipe flow), the physical mechanisms governing migration should be the same. To check the prediction of simulation in this regime of sedimentation we used less viscous liquid in our two-dimensional channels to observe the settling at higher Reynolds numbers. The trajectory of the sphere in the two-dimensional channel at $Re = 256.9$ (figure 22*a*) looks like the prediction of our two-dimensional simulation at $Re = 8.33$ in figure 7. The same sequence of dynamics is observed in two-dimensional simulations and three-dimensional motions in two-dimensional beds, but the Reynolds numbers in the experiments are much higher and the intervals of Reynolds numbers in which a given dynamics is prevalent are also larger in the experiments.

The rocking motion corresponding to our regime D has been reported in the literature in pipe flow. Foster, Hair & Doig (1975) recorded the motion of spherical particles suspended in a pipe flow and identified four different regimes. In their regime D, covering a particle Reynolds number range of 200 to 10000, the particles oscillate steadily in the radial direction around a mean equilibrium position close to the wall. This description is in good agreement with our simulation in the high-Re regime. In our two-dimensional channel, we also observed the typical behaviour of persistent oscillation. A trajectory recorded by video-taping is shown here (figure 22*b*). Note that

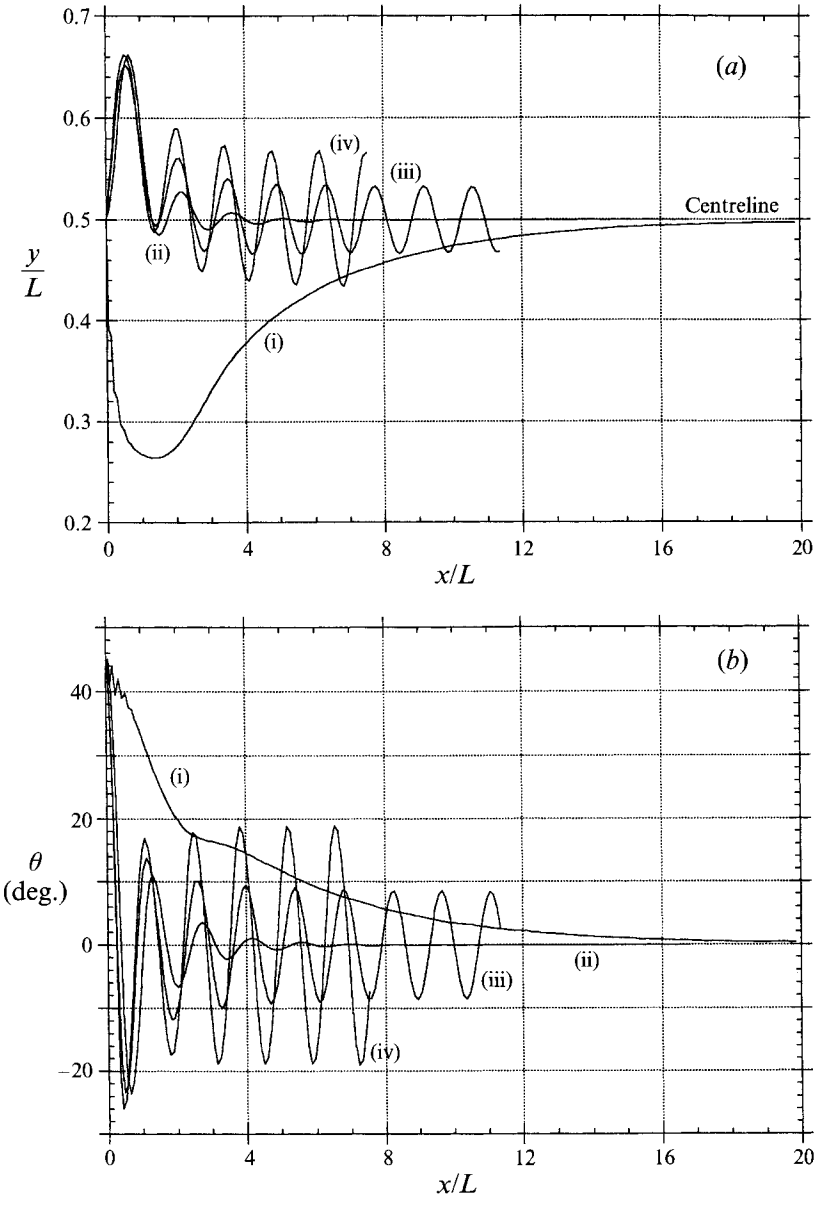

FIGURE 24. Sedimentation of a 2:1 elliptic cylinder in a channel of width $L = 4d$, d being the length of the major axis. (*a*) Lateral position of the centre of the ellipse (y/L), initial $y_0 = 0.5L$. (*b*) Orientation of the ellipse (when the major axis is horizontal, $\theta = 0$), initial $\theta_0 = 45°$. (i) $Re = 2.0$, (ii) $Re = 12.8$, (iii) $Re = 26.7$, (iv) $Re = 35.7$.

this time the Reynolds number is actually in our simulated high-Re regime. This is in contrast to the lower-Re regimes, where the two-dimensional channel gives the same behaviour at much higher Re. This shows that the effects of close sidewalls in a two-dimensional channel are complicated and depend on the Reynolds number.

Finally, let us consider the last regime of motion. Tachibana (1973) briefly mentioned that when the terminal $Re = 500 \sim 750$, the settling sphere experiences an irregular and complex motion, and often in three dimensions. This is the only verification of our irregular oscillation regime simulations that we could find in the

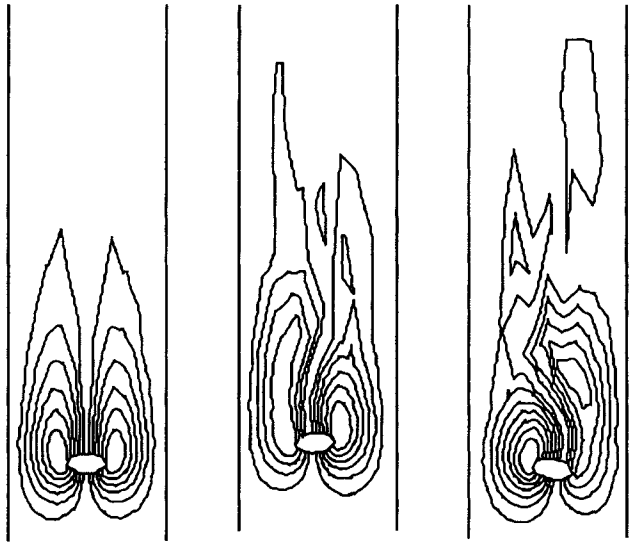

FIGURE 25. Streamlines around a 2:1 elliptic particle at different Reynolds numbers.

literature. In our two-dimensional channels, sedimentation tests indeed reveal irregularity in the lateral rocking motion when Re is large enough. Figure 23 shows a typical trajectory of a short cylinder in our wide channel.

In summary, the regimes of flow predicted by two-dimensional simulations appear in experiments in which spheres and short cylinders sediment between close walls. The sequence of regimes is the same in the simulations and experiments, but the values of the Reynolds number defining the regimes can be much different in a non-uniform way.

4. Settling of an elliptic particle between parallel walls

The orientation of a sedimenting elliptical particle is of interest. Inertia is important because it gives rise to a turning couple on the particle that determines a preferred orientation.

4.1. *Reynolds-number regimes*

The settling behaviour of an elliptic particle can be classified into four different Re regimes in very much the same fashion as in last section. Figure 24 shows typical trajectories and orientations of a 2:1 ellipse for different Reynolds numbers.

The lateral motion and rotation are very similar and closely related. If the Reynolds number is below a critical value, which can be roughly estimated as around 25, the particle eventually settles steadily. The final equilibrium position is at the centre of the channel, obviously due to the same wall effects which force circular cylinders to the channel centre, and the preferred orientation is with the major axis perpendicular to the direction of the settling. This is a well-known result of potential flow theory (Lamb 1932, pp. 174–177) which has been generalized to viscous flow by Huang, Feng & Joseph (1994). The approach to this final configuration does not overshoot at small Reynolds numbers ($Re = 2$, say), although there is a big hump in the lateral motion because of a lift force related to the initial orientation of the body. At larger Re, the inertia is stronger and causes overshoot in both y and θ ($Re = 12.8$). This initial oscillation is still an inertial effect which is damped by viscosity after a few cycles. At still larger Re, this oscillation becomes persistent, and is apparently identical to the

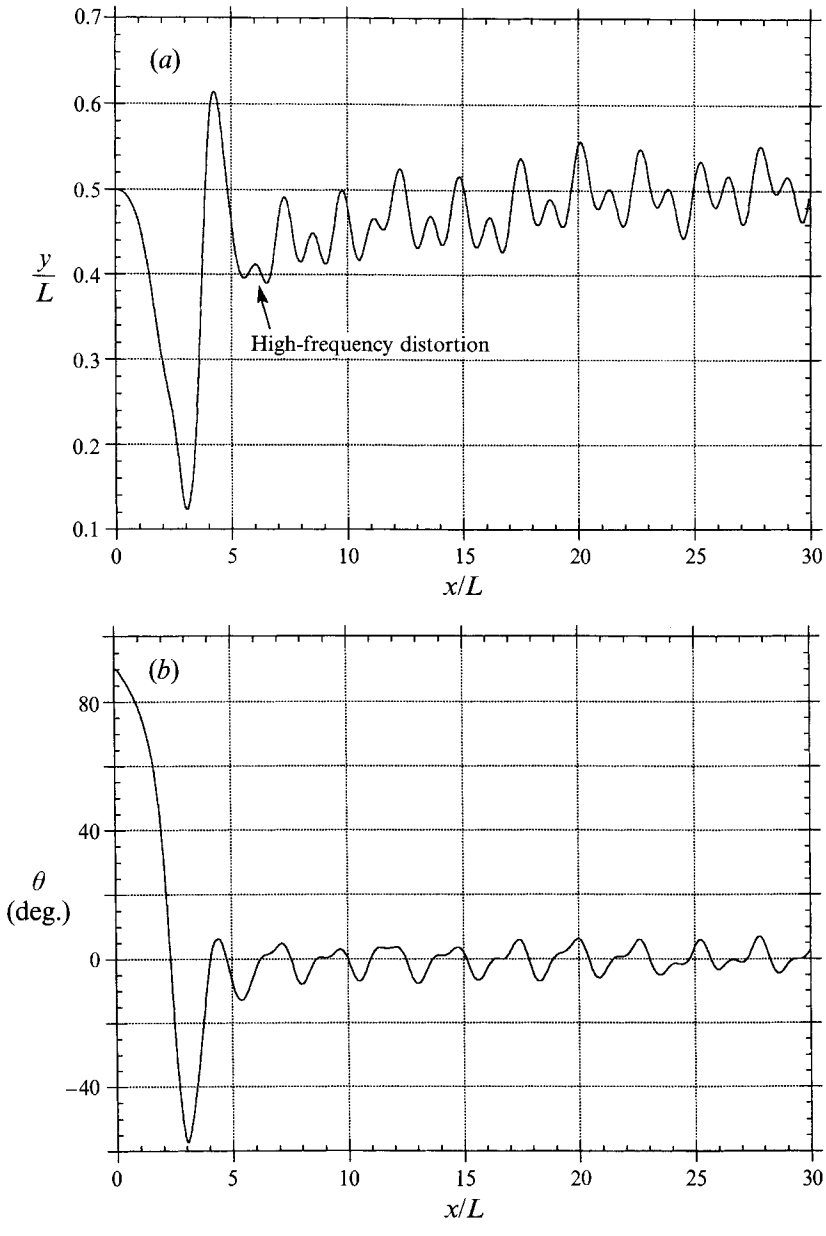

FIGURE 26. Sedimentation of a 1.1:1 elliptic cylinder in a channel of width $L = 4d$ at $Re = 345$. (*a*) Lateral position y, initial $y_0 = 0.5L$; (*b*) angular position θ, initial $\theta_0 = 90°$.

zigzag motion of a rising bubble in a liquid (Saffman 1956; Hartunian & Sears 1957). As for the driving force that sustains the oscillation, Jayaweera & Mason (1965) pointed to vortex shedding. But streamlines in our calculation (figure 25) suggest that prior to vortex shedding, the periodic 'swing' of the attached eddies is enough to maintain the oscillation ($Re = 26.7$), which is supported at higher Re by the stronger side-ways action of vortex shedding ($Re = 35.7$: this value is very close to the critical Re predicted by Jackson (1987) for the onset of vortex shedding behind a 2:1 ellipse). This verifies Saffman's (1956) surmise that the zigzag pattern of a rising bubble is caused by 'an oscillation in the wake or a periodic discharge of vorticity from behind

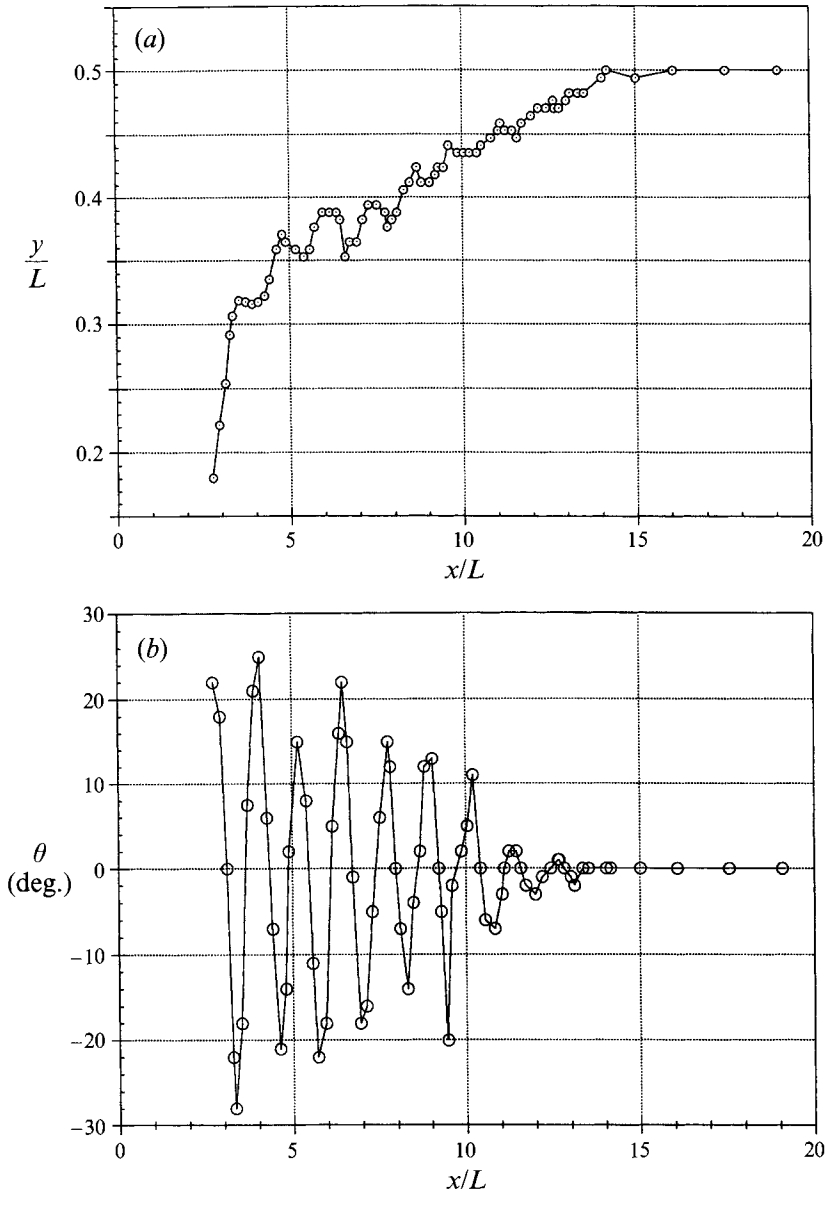

FIGURE 27. Sedimentation of a 2:1 elliptic cylinder in the wide 'two-dimensional' channel at $Re = 694.7$. (*a*) Lateral position of the centre of the ellipse; (*b*) orientation of the cylinder ($\theta = 0$ is with long axis horizontal).

the bubble'. It is interesting to note that the rocking and oscillating particle does not drift off the centre of the channel as a circular particle does. This is related to the fact that as long as the body does not tumble, an enduring rotation in one sense is not possible. This is further illustrated by a high-*Re* calculation shown in figure 26. Even for aspect ratios as small as 1.1 and *Re* as high as 345, the broadside-on effect prevents the ellipse from tumbling. Thus, although the inertial action initially moved the particle far enough from the centreline, no lift force sustains this position and the particle is gradually pushed back to the centreline by the wall effect. This is strong support for the mechanism proposed in §3.2, in which a rotation-induced lift is the agent

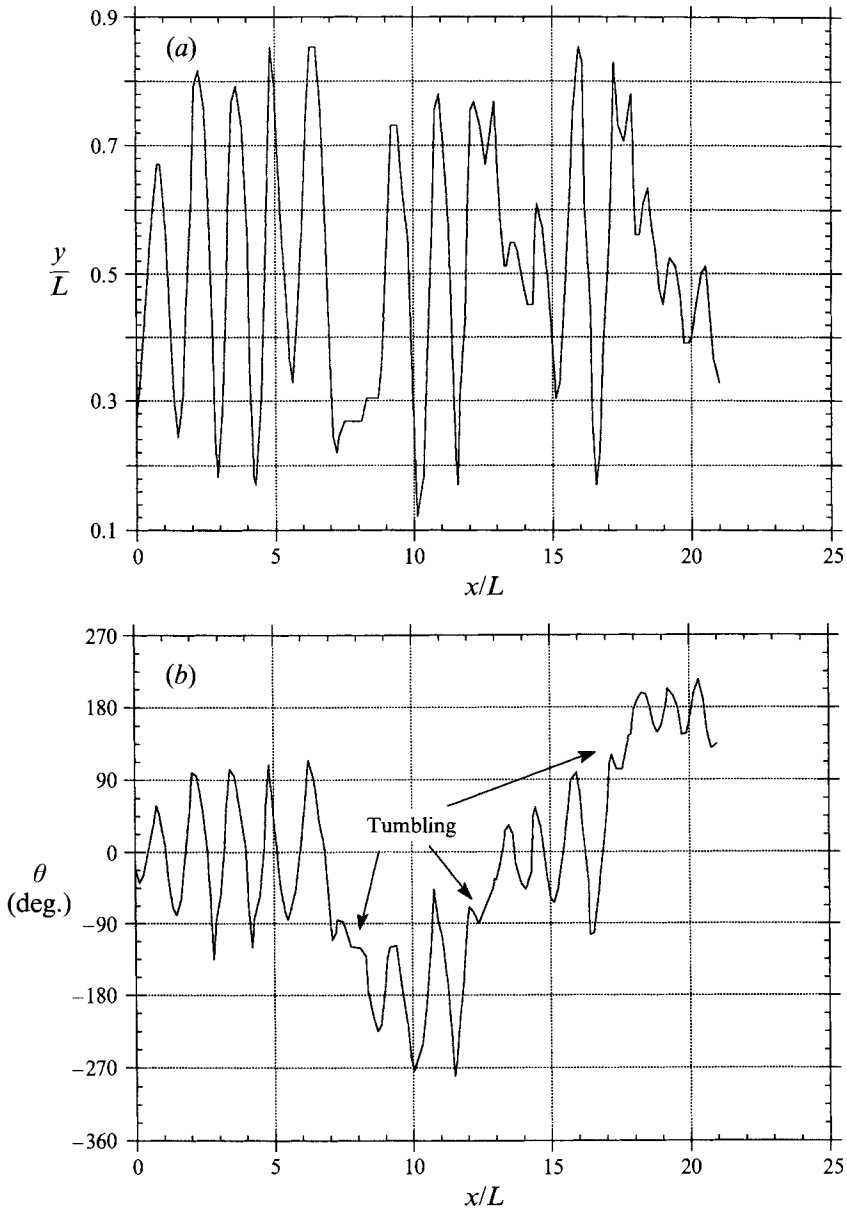

FIGURE 28. Sedimentation of a 2:1 elliptic cylinder in the narrow 'two-dimensional' channel at $Re = 666.9$. (*a*) Lateral position of the centre of the ellipse; (*b*) orientation of the cylinder ($\theta = 0$ is with major axis horizontal).

destabilizing the equilibrium at the centreline. Another interesting feature in figure 26 is the distortion in the oscillatory motion. An examination of the flow field (streamlines, vorticity and pressure distribution) around the particle at different time steps reveals that the small wiggles are caused by periodic vortex shedding. The oscillation of lower frequency is due to the inertial lift and torque associated with the orientation of the particle, and will eventually be damped out by viscosity.

Jayaweera & Mason (1965) have made the only systematic observations and measurements of settling cylindrical particles, which possess the same geometric

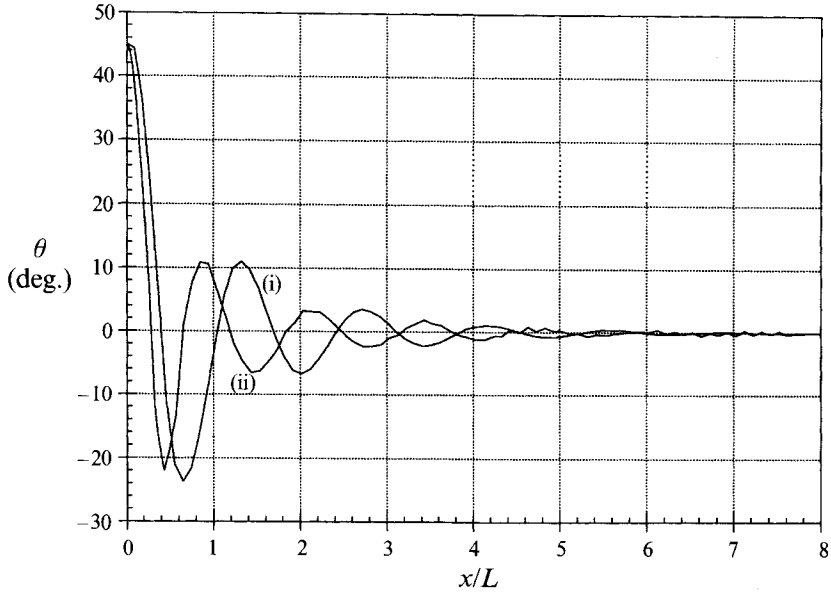

FIGURE 29. Effect of aspect ratio of elliptic cylinders on their sedimentation in a vertical channel, $\theta = 0$ is with the major axis horizontal. Initial $\theta_0 = 45°$. (i) Aspect ratio 2:1, $Re = 12.8$; (*ii*) aspect ratio 4:1, $Re = 16.6$.

features as our two-dimensional elliptic particle. Their description of the low-Re steady motion, the damped oscillatory motion and finally the persistent fluttering motion is in perfect agreement with the simulations given here. Especially, they recognized the broadside-on mode as the stable orientation if Re is below a certain value, and believed that vortex shedding is the reason for the subsequent regime of persistent oscillation, which may not be entirely true as suggested by the simulation at $Re = 26.7$.

As an independent verification, we studied the sedimentation of ellipsoids of aspect ratio 2:1 in our 'two-dimensional' channels. Despite geometric differences, essentially the same behaviour is observed. Figure 27 shows how the equilibrium at the centreline is approached in the wide channel ($L = 8d$). Figure 28 shows high-Re oscillatory behaviour in the narrow channel when sporadic tumbling starts during the fluttering sedimentation. Three interesting points should be noted from these two figures. First, the Reynolds numbers for experiments in our two-dimensional channels are much larger than Re in our simulation. Jayaweera & Mason's test in a large tank gives threshold Re values comparable with our numerical results after making the required two-/three-dimensional Re conversion. We again see that the influence of the bounding walls on the particle motion in the 'two-dimensional' channel is complex and that it seems to affect the motion in the vertical and horizontal directions differently. Besides, our experiments indicate that the unsteadiness in the settling is enhanced by wall effects in a narrow channel. Finally, a careful study of figure 28(*a*, *b*) shows that tumbling corresponds to (temporary) off-centre positioning of the particle. This again supports our argument about the tumbling and off-centre drift made in explanation of figure 26.

4.2. *Other effects*

The aspect ratio is also a factor in determining how an ellipse settles. Jayaweera & Mason (1965) concluded that at the same Re, the motion of shorter particles is always more apt to be unsteady. The larger the aspect ratio, the higher Re has to be to realize the constant fluttering mode of motion. This may appear at first glance to contradict

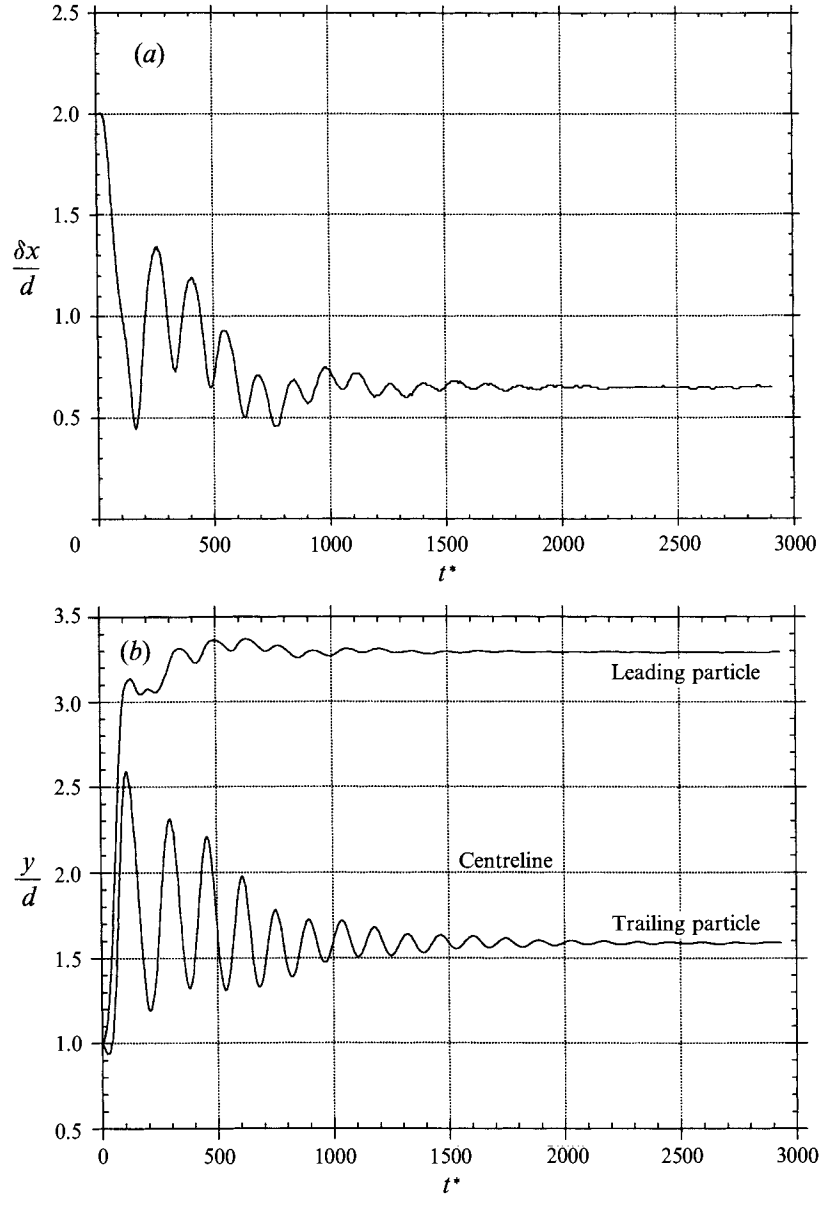

FIGURE 30(*a*, *b*) For caption see facing page.

the fact that the critical *Re* for vortex shedding from an ellipse is smaller if the ellipse is thinner in the direction of the stream (Jackson 1987). But the motion of a free particle depends on more than the flow field around it. For example, the motion of a longer particle induces a larger added mass and an especially larger added moment of inertia, and therefore is more stable in its reaction to outside forces and torques. We tried to simulate this mechanism, and the effect seems not to be as pronounced as in the experiments of Jayaweera & Mason. In figure 29, we show that the reaction of a 4:1 elliptic cylinder at higher *Re* is not quite as strong as a 2:1 ellipse at smaller *Re*.

Another fact that deserves mentioning is that the inertia (and moment of inertia) of the particle itself is as influential as that of the fluid. In our simulation we have noticed,

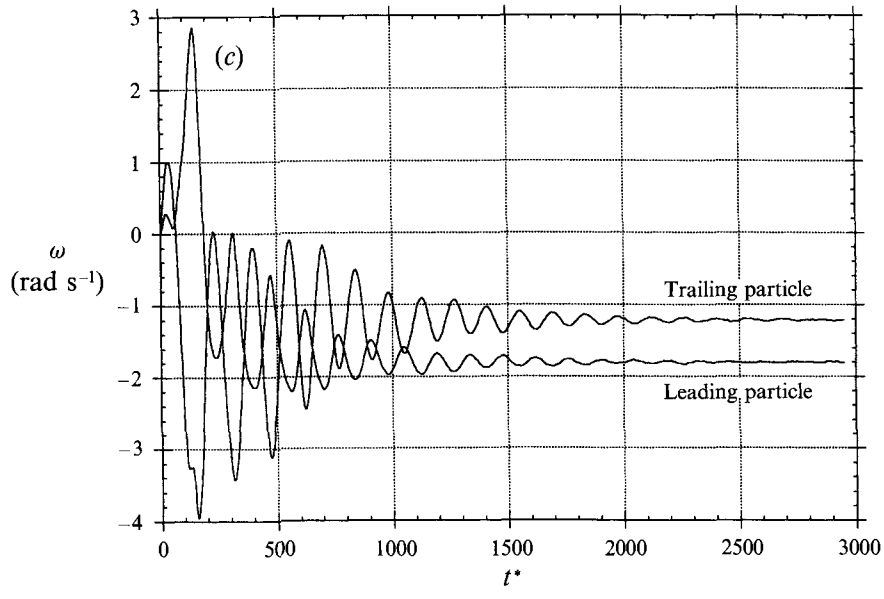

FIGURE 30. The sedimentation of two circular particles in a $4d$ channel. Final $Re = 2.87$. The dimensionless time $t^* = t(g/d)^{\frac{1}{2}}$. (*a*) Vertical distance between particles, (*b*) particle positions in the horizontal direction, (*c*) angular velocity (negative ω corresponds to clockwise rotation).

for example, that a lighter particle rising in the fluid is more active than a heavier particle settling at the same Re. One implication is that the specification of Re plus geometry is not sufficient to identify the motion of a free body. We have not in this paper carried out systematic studies of the inertia of the particle.

5. Interaction of two particles settling in a channel

Joseph *et al.* (1987) and Fortes *et al.* (1987) discovered that the basic mechanisms controlling the motion and interactions of spherical bodies at moderately high Reynolds numbers are associated with wakes and turning couples on long bodies. This was described by them as drafting, kissing and tumbling (DKT). A dynamic simulation of DKT was given by Hu *et al.* (1992*b*) at $Re = 30$ and 100. In this section, we will study the motion and interaction of two particles settling in a two-dimensional channel at various Reynolds numbers. Two circular particles of diameter d are released in a vertical channel of width L and then settle under gravity. Two channel widths are used: $L = 4d$ and $8d$. The initial positions of the particles are midway between the centreline of the channel and one wall, with one particle $2d$ behind the other, except in one case in which we started two particles horizontally aligned, $2d$ apart across the centreline (figure 32).

5.1. *Steady solutions*

At low Reynolds numbers, there is an attracting steady solution in which two particles settle in a staggered structure with constant velocity. A typical run in a $4d$ channel with final $Re = 2.87$ is shown in figure 30(*a–c*). The particles are initially midway between the centreline and one wall, with one particle $2d$ behind the other. After release, the trailing particle accelerates into the wake of the leading particle. After a close approach, the trailing particle turns around the leading one without touching it. After this, the particles enter a damped oscillation. Figure 30(*a*) shows the variation of the

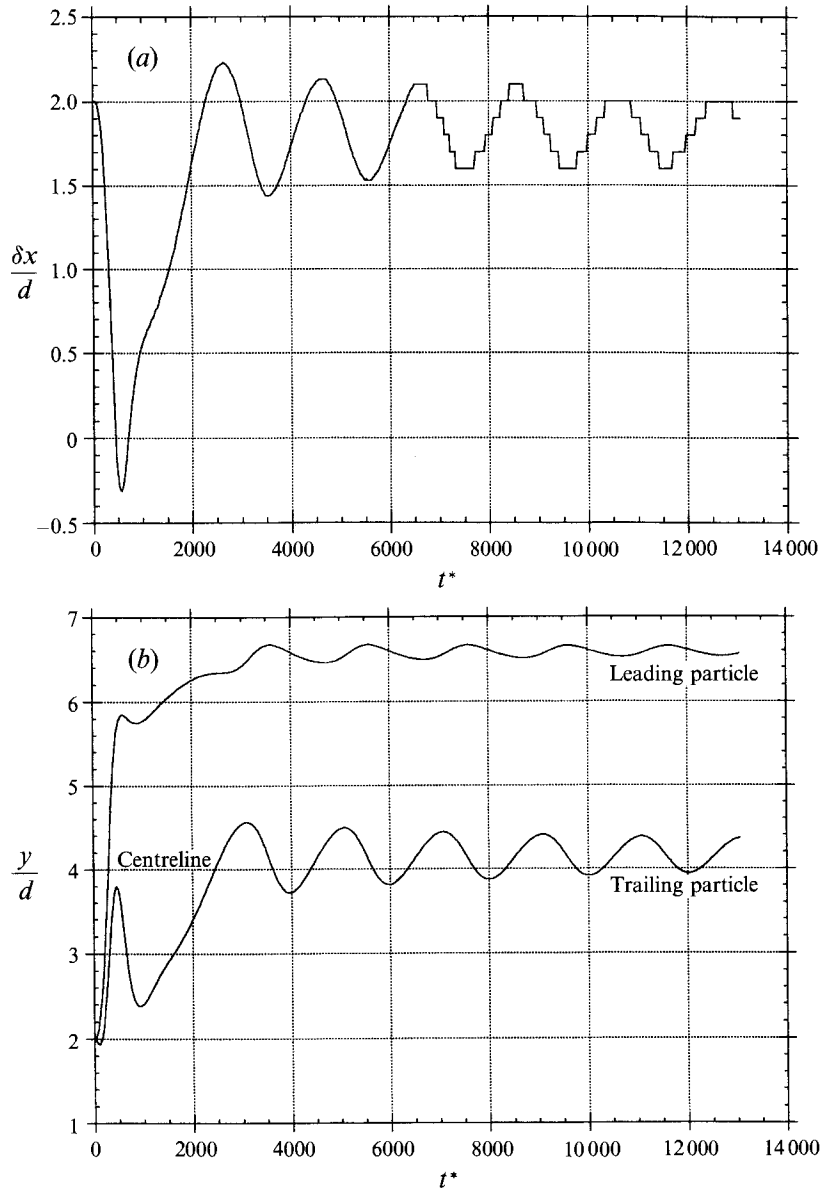

FIGURE 31 (a, b) For caption see facing page.

vertical distance between the particles. In the lateral motion (figure 30b), the leading particle is closer to one wall and oscillates with smaller amplitude than the trailing particle. The angular velocity of both particles oscillates also (figure 30c), the trailing particle with a larger amplitude.

The oscillation is mostly damped by viscosity before $t^* = 2000$, and a perfectly stable equilibrium configuration is attained in which the two particles are staggered and settle with constant velocity. The particles rotate in the same sense and the trailing particle rotates slower than the leading one in this particular case.

A similar simulation was performed in an $8d$ channel in which the final Reynolds number was $Re = 1.52$, and the results are shown in figure 31 (a–c). The initial transient

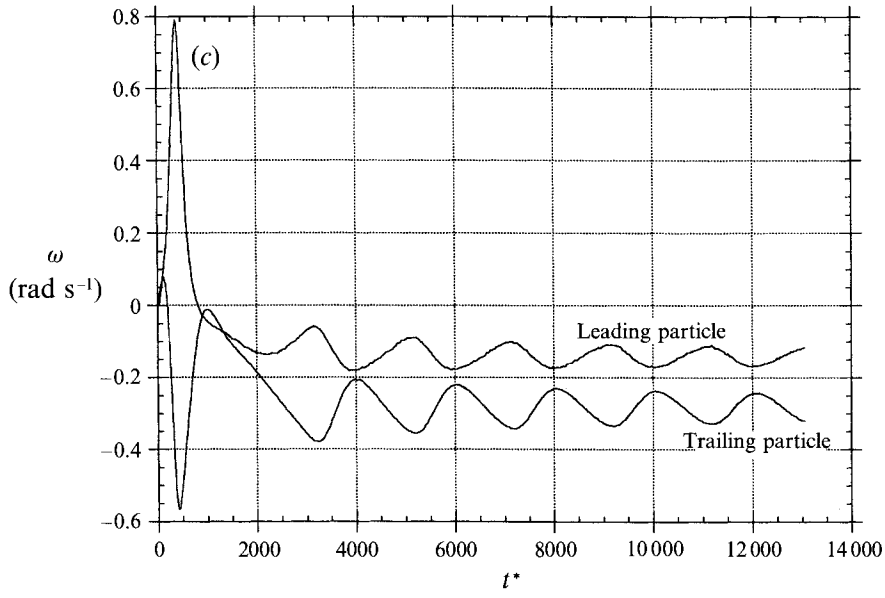

FIGURE 31. The sedimentation of two circular particles in an $8d$ channel. Final $Re = 1.52$. (*a*) Vertical distance between particles, (*b*) particle positions in the horizontal direction, (*c*) angular velocity (negative ω corresponds to clockwise rotation).

is the same as in the last run. After that, the viscous damping is much weaker even though the Reynolds number is smaller than in the $4d$ channel. The frequency of oscillation is also smaller. The two particles rotate in the same sense, and the trailing particle rotates faster than the leading particle. We did not continue the computation to the final steady state because of the high cost of computing slow decay. But it is clear that the amplitude of oscillation decreases monotonically, and a stable staggered structure should eventually be achieved. The small wiggles in $\delta x/d$ are a numerical effect caused by using large time increments in explicitly updating the particle positions.

The characteristic behaviour of two particles settling in a channel at low Reynolds numbers can be compared with the low-Re settling of two cylinders in a very large container. The two-cylinder problem was studied in the experiments of Jayaweera & Mason (1965) who found that the trailing particle would first accelerate toward and then turn around the leading one, in much the same way as described here. Then they would align in a horizontal line and separate while settling. A similar interparticle repulsion was discovered by Kim *et al.* (1993) in a three-dimensional flow past two spheres. In a two-dimensional fluidized bed, Joseph *et al.* (1987) and Fortes *et al.* (1987) observed that particles form stable cross-stream arrays. The results of our simulation are consistent with these observations. However, the channel walls appear to have a stronger influence in the simulation than in the experiment. The walls tend to push the particles together and their mutual repulsion keeps them apart. The competition is resolved with a staggered rather than cross-stream arrangement in the channel. In the experiments of Joseph *et al.* (1987), the cross-stream arrays also tend to bend slightly close to the walls.

The same solution arises from a different initial condition in which two particles are released from a horizontal line (figure 32*a–c*). Before $t^* = 1000$, the particles settle

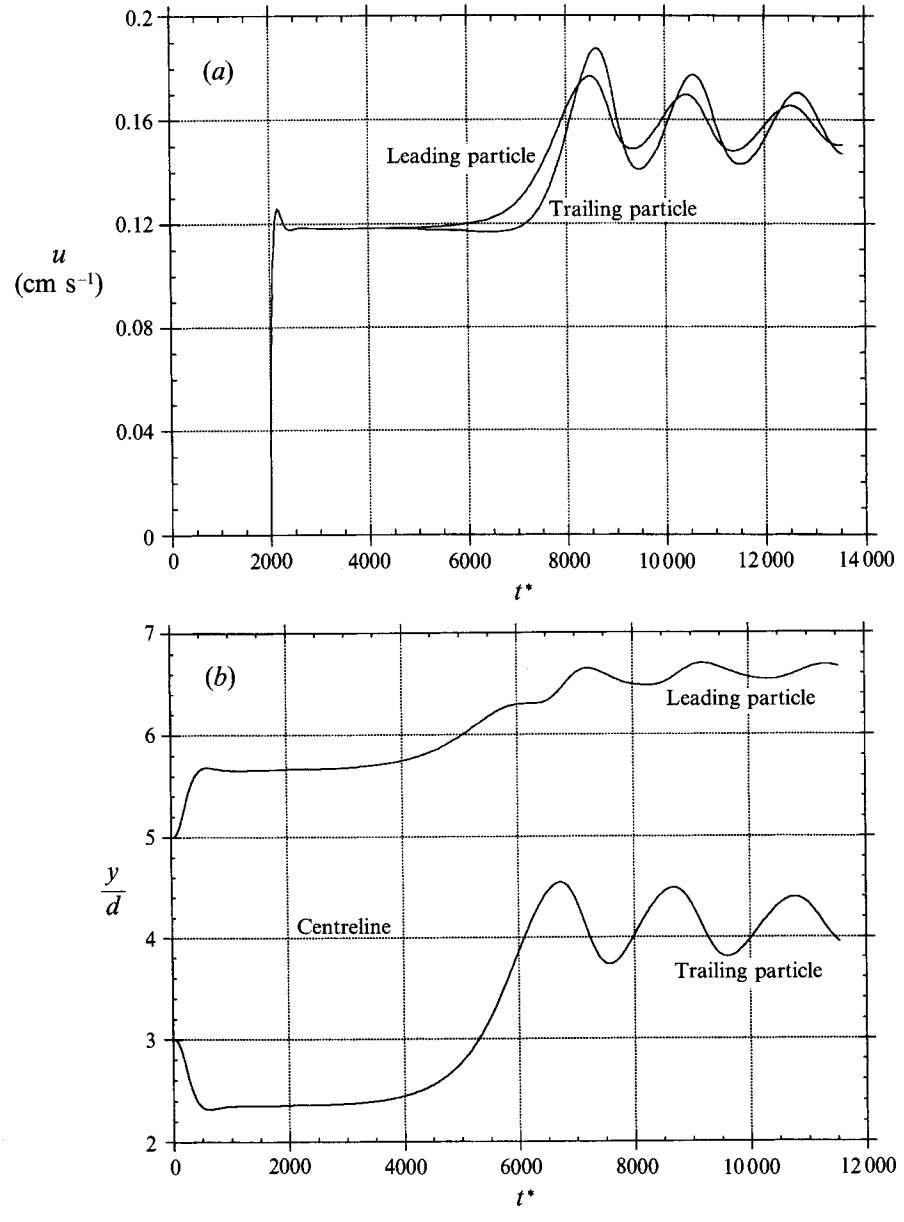

FIGURE 32(*a*, *b*) For caption see facing page.

symmetrically while separating and rotating in different senses in just the way described by Jayaweera & Mason (1965). Then the separation and rotation stop and a steady horizontal structure appears for a time ($1000 < t^* < 3000$). But soon wall repulsion ruins the symmetry and pushes one particle to the centreline, slowing it down at the same time. This leads to the same damped oscillation as shown in figure 31. The transition from different initial conditions to the final staggered structure in our two-dimensional simulation suggests that the staggered structure is an attractor.

Hydrodynamic interactions between particles and walls are stronger in a narrower channel. In our $4d$ channel, the oscillation frequency is higher and the damping is

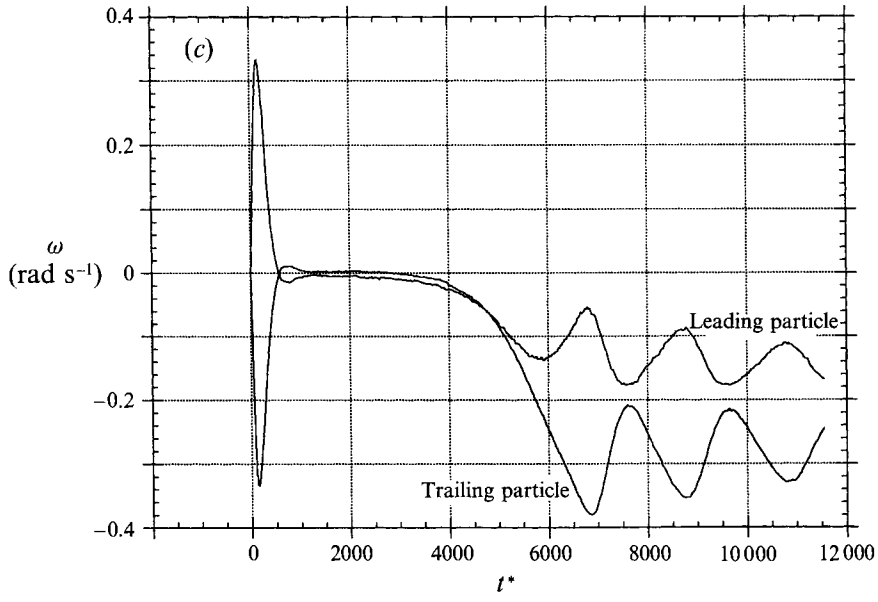

FIGURE 32. The sedimentation of two circular particles in an $8d$ channel. Initially the particles are on the same horizontal line. Final $Re = 1.52$. (*a*) Vertical velocity component, (*b*) particle positions in the horizontal direction, (*c*) angular velocity (negative ω corresponds to clockwise rotation).

faster. The angle between the line of centres and the horizontal is smaller and the particles are less staggered than in an $8d$ channel.

The rotation of the leading particle is such that it seems to be rolling up the nearby wall. This is similar to the low-Re settling of a single particle. The trailing particle experiences a strong downward stream on its right side due to the wake of the leading one (figure 33). This asymmetry of the flow on both sides of the trailing particle results in a remarkable rotation in the same sense as that of the leading particle. In the $4d$ channel (figure 30), the trailing particle is on the opposite side of the channel to the leading one, and rotates slower than the leading particle. In the $8d$ channel (figure 31), the trailing particle is near the centreline and rotates faster than the leading one. Rotation influences the staggered structure by inducing a Magnus type of lift on both particles, which balances the wall repulsion and interparticle repulsion to maintain a stable configuration.

5.2. *Periodic solutions*

At larger values of the Reynolds number, the staggered steady structure bifurcates into a periodic motion, due primarily to effects of the wake. The motion and rotation of two particles settling at average Reynolds number $Re = 3$ are shown in figure 34. The vertical distance between the particles varies periodically. The trailing particle oscillates around the centreline and the leading one oscillates around a line closer to one wall. They rotate in the same sense with angular velocities which vary periodically after an initial transient. The trailing particle rotates faster than the leading one. This difference in speed may be interpreted by the reasoning given at the end of § 5.1. The interaction between particles is illustrated by the series of snapshots of the particle motion shown in figure 35. Suppose that in the early stage of settling, a staggered structure is formed (figure 35*a*i). The trailing particle is pulled into the wake of the leading particle (figure 35*a*ii). When the particles get close enough, interparticle repulsion throws the trailing particle out of the wake (figure 35*a*iii, iv). Now the simultaneous action of wall

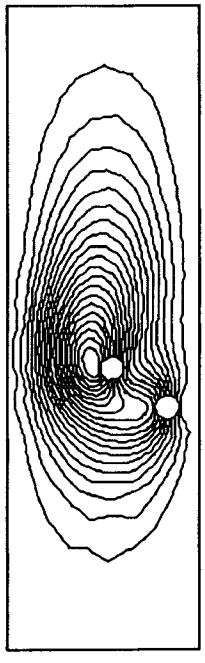

FIGURE 33. Streamlines for the settling of two particles at $Re = 1.52$ in an $8d$ channel. Note that the wake of the leading particle causes the trailing particle to rotate clockwise.

repulsion, interparticle repulsion and lift due to rotation tends to restore the original staggered structure by slowing down the trailing particle and increasing the vertical separation (figure 35*a* v, vi). Then the entire process will repeat. The addition of wake suction to the force balance in the horizontal direction, which would maintain a steady staggered structure at a lower Re, causes the periodic vertical manoeuvre.

The wake suction induces a persistent oscillation in the motion and rotation of the particles. Numerical tests show that the frequency and amplitude of the oscillation increase with the Reynolds number. We also note that for larger Reynolds number, the mean position of the trailing particle is swept further behind, and the angle that the line of centres between particles makes with the vertical wall becomes smaller (figure 36).

5.3. *Drafting, kissing and tumbling*

At even larger Reynolds numbers, the interaction between particles assumes a more active pattern. The trailing particle is sucked into the wake of the other, and drafted toward it with increasing velocity. Then they almost touch ('kissing', see figure 35*b* ii: the distance between centres at this moment is $1.013d$). Because the configuration with the doublet standing vertically is unstable, it tumbles and the top particle turns around the bottom particle to take the lead (figure 35*b* iii, iv). The particle near the wall gains a small upward velocity and is ejected with a large lateral velocity to the sidewall (figure 35*b* iv). After a time, this particle moves away from the wall and is again attracted to the wake of the leading particle (figure 35*b* v) and the cycle is repeated. At this Reynolds number, the two particles never come into actual contact. When they are close, the lubrication layer between them provides a high enough pressure to keep them apart. At higher Reynolds numbers, the inertia of particles becomes strong enough and they tend to collide. The meshing program breaks down at this moment.

In summary, the most important factors in the interaction among settling particles

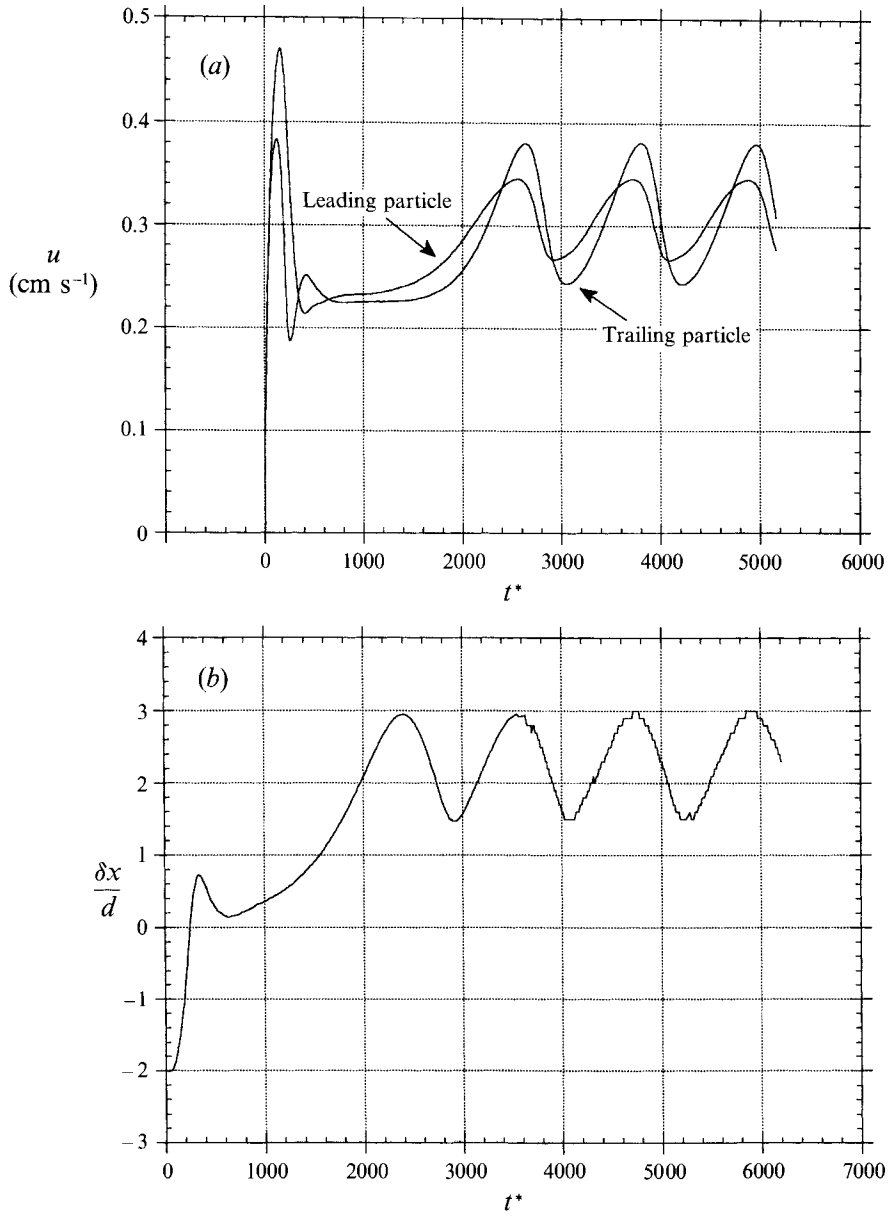

FIGURE 34(*a*, *b*) For caption see page 130.

are interparticle repulsion and wake suction. If walls are present, they impose lateral forces to modify the motion of particles. Reynolds number influences the motion and interaction of particles gradually.

As mentioned before, the numerical simulations at small and large Reynolds numbers are consistent with experimental observations (Jayaweera & Mason 1965; Joseph *et al.* 1987). But we cannot simulate the stably locked structure discovered by Fortes & Joseph (1992) at intermediate Reynolds numbers. Their experiment was performed using spheres in a two-dimensional fluidization apparatus. The particles are confined to move in a plane. For $22 < Re < 43$, a cluster of up to four particles are arranged in a stable staggered structure. At *Re* out of this range (either larger or

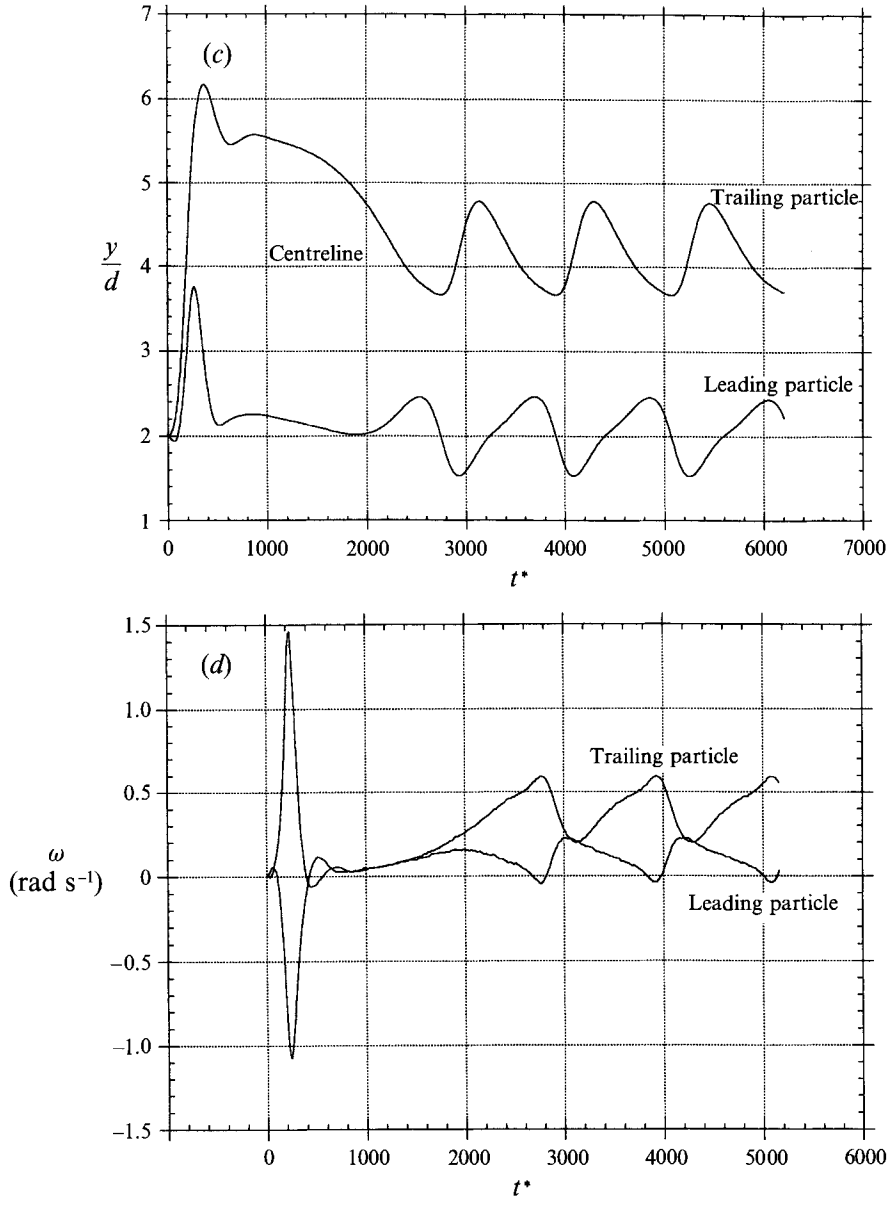

FIGURE 34. The sedimentation of two circular particles in an $8d$ channel. Final $Re = 3$. (*a*) Vertical velocity component, (*b*) vertical distance between particles, (*c*) particle positions in the horizontal direction, (*d*) angular velocity (positive ω corresponds to counterclockwise rotation; note that the leading particle is close to the left wall).

smaller), the usual DKT behaviour prevails. Our two-dimensional simulation predicts a gradual transition as Re increases. Thus, the observed stably locked structure is probably caused by the two walls that are very close to the particles. The peculiar wall effect in a 'two-dimensional' apparatus of this type has been discussed in §§3.5 and 4.1 as associated with sedimentation of single circular and elliptic particles.

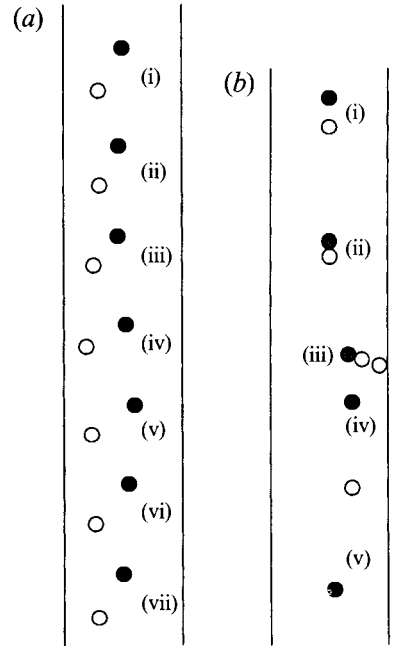

FIGURE 35. (*a*) The interaction between two particles settling in an $8d$ channel at $Re = 3$. (i) $t = 24.01$ s, (ii) $t = 25.89$ s, (iii) $t = 27.49$ s, (iv) $t = 29.43$ s, (v) $t = 31.62$ s, (vi) $t = 33.64$ s, (vii) $t = 35.6$ s. (*b*) The interaction between two particles settling in an $8d$ channel at $Re = 70$. (i) $t = 0$, (ii) $t = 1.634$ s, (iii) $t = 2.518$ s, (iv) $t = 3.023$ s, (v) $t = 5.3735$ s.

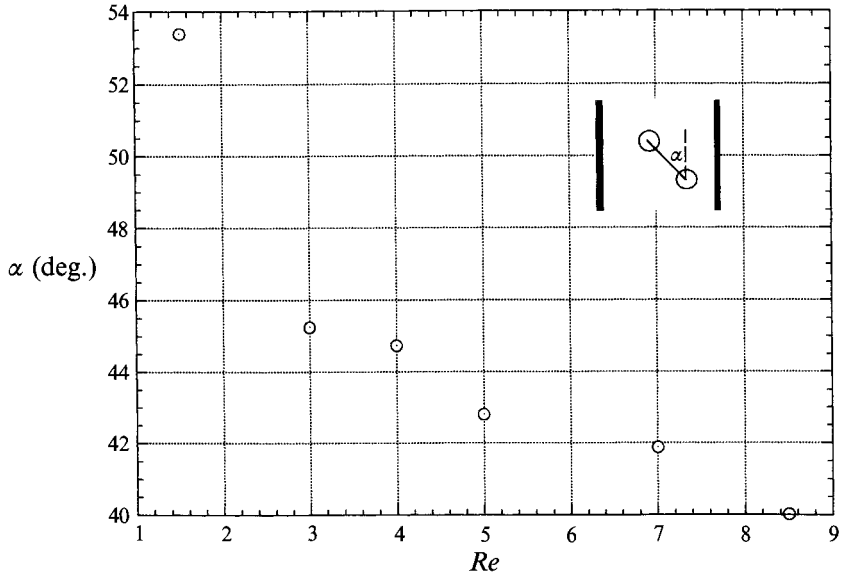

FIGURE 36. The mean relative position of the settling particles at various Reynolds numbers. The channel width $L = 8d$.

6. Conclusions

Based on the results and discussions presented in this paper, the following conclusions can be drawn for the parameter ranges covered in this study.

(i) A circular particle settling in a vertical channel can be said to experience five

different regimes of motion at different Reynolds numbers, which are closely related to the wake structure behind the particle. When Re is small, the particle migrates to a steady equilibrium at the centre of the channel. This steady motion bifurcates into a oscillatory motion at a critical Reynolds number, and the mean equilibrium position is moved off the centreline toward one wall. At higher Reynolds numbers, this periodic motion is unstable and gives way to irregular motion.

(ii) Channel walls affects the sedimentation of a particle. The Reynolds number intervals in which a certain regime occurs vary if the channel width changes. Walls also increase the drag coefficient of a settling particle. Particles are always kept a certain distance away from the wall by a repulsion. This effect can be of significance in the transportation of particulate mixtures.

(iii) A settling elliptic particle exhibits similar regimes of motion at different Reynolds numbers. At small values of the Reynolds number, steady settling is ultimately achieved. When vortex shedding occurs, persistent rocking motion prevails. Since tumbling is difficult for an elliptic cylinder, the mean equilibrium position does not deviate from the centreline.

(iv) The interaction of two particles settling in a channel gives rise to different regimes of motion. Bifurcation of the steady solution to periodic solution occurs at low Reynolds number without vortex shedding. This is a particle system bifurcation rather than a fluid bifurcation. The drafting–kissing–tumbling scenario is realized at higher Reynolds numbers.

(v) The results of our two-dimensional simulations are in good qualitative agreement with experiments on sedimentation and fluidization of spheres and long particles confined to move in two dimensions by close walls. No universal rule for quantitative comparisons of two-dimensional simulations with three-dimensional flow has been found.

Finally, we note that our fully nonlinear simulations discovered features of the particle motion previously unknown in perturbation theories, such as the bifurcation and drift away from the centreline.

This work was supported by the NSF Fluid, Particulate and Hydraulic Systems, by the US Army Mathematics and AHPCRC, by the DOE Department of Basic Energy Sciences and the Minnesota Supercomputer Institute. H.H.H. acknowledges the partial support from the NSF through Laboratory for Research on the Structure of Matter at the University of Pennsylvania and from the Research Foundation of the University of Pennsylvania. The authors wish to thank Mr R. Bai for his assistance in the sedimentation experiments, and Mr Adam Huang for helpful discussions.

REFERENCES

ANDERSON, T. B. & JACKSON, R. 1967 A fluid mechanical description of fluidized beds: Equations of motion. *Ind. Engng Chem. Fundam.* **6**, 527–539.

APELT, C. J. 1961 The steady flow of a viscous fluid past a circular cylinder at Reynolds numbers 40 and 44. *Aero. Res. Counc. R. & M.* 3175.

BATCHELOR, G. K. 1974 Transport properties of two-phase materials with random structure. *Ann. Rev. Fluid Mech.* **6**, 227–255.

BRADY, J. F. & BOSSIS, G. 1985 The rheology of concentrated suspension of spheres in simple shear flow by numerical simulation. *J. Fluid Mech.* **155**, 105–129.

BRENNER, H. 1966 Hydrodynamic resistance of particles at small Reynolds numbers. *Adv. Chem. Engng* **6**, 287–438.

DENSON, C. D., CHRISTIANSEN, E. B. & SALT, D. L. 1966 Particle migration in shear fields. *AIChE J.* **12**, 589–595.

DREW, D. 1983 Mathematical modeling of two-phase flow. *Ann. Rev. Fluid Mech.* **15**, 261–291.

FEUILLEBOIS, F. 1989 Some theoretical results for the motion of solid spherical particles in a viscous fluid. In *Multiphase Science and Technology*, Vol. 4 (ed. G. F. Hewitt *et al.*), pp. 583–789. Hemisphere.

FORNBERG, B. 1980 A numerical study of steady viscous flow past a circular cylinder. *J. Fluid Mech.* **98**, 819–855.

FORTES, A. F. & JOSEPH, D. D. 1992 Wake architectures in two-dimensional fluidization of spheres: experiments and phenomenological description. *Proc. DOE/NSF Workshop on flow of particulates and fluids, Worcester, MA, October 22–24, 1991.*

FORTES, A. F., JOSEPH, D. D. & LUNDGREN, T. S. 1987 Nonlinear mechanics of fluidization of beds of spherical particles. *J. Fluid Mech.* **177**, 467–483.

FOSTER, B. P., HAIR, A. R. & DOIG, I. D. 1975 Suspension of spheres in fully developed pipe flow. *Chem. Engng J.* **9**, 241–249.

GERRARD J. H. 1978 The wakes of cylindrical bluff bodies at low Reynolds number. *Phil. Trans. R. Soc. Lond.* A **288**, 351–382.

HAPPEL, J. & BRENNER, H. 1965 *Low Reynolds Number Hydrodynamics.* Prentice-Hall.

HARTUNIAN, R. A. & SEARS, W. R. 1957 On the stability of small gas bubbles moving uniformly in various liquids. *J. Fluid Mech.* **3**, 27–47.

HASSONJEE, Q., PFEFFER, R. & GANATOS, P. 1992 Behavior of multiple spheres in shear and Poiseuille flow fields at low Reynolds number. *Intl J. Multiphase Flows.* **18**, 353–370.

HOCKING, L. M. 1964 The behaviour of clusters of spheres falling in a viscous fluid. Part 2 slow motion theory. *J. Fluid Mech.* **20**, 129–139.

HONJI, H. 1972 Starting flows past spheres and elliptic cylinders. *Rep. Res. Inst. Appl. Mech., Kyushu Univ.* **19**, 271–281.

HU, H. H., FORTES, A. F. & JOSEPH, D. D. 1992*a* Experiments and direct simulations of fluid particle motion. *Video J. Engng Res.* **2**, 17–24.

HU, H. H., JOSEPH, D. D. & CROCHET, M. J. 1992*b* Direct simulation of fluid particle motions. *Theoret. Comput. Fluid Dyn.* **3**, 285–306.

HUANG, Y., FENG, J. & JOSEPH, D. D. 1994 The turning couple on an elliptic particle settling in a vertical channel. *J. Fluid Mech.* (to appear).

ISHII, M. 1975 *Thermo-Fluid Dynamic Theory of Two-Phase Flows.* Eyrolles.

JACKSON, C. P. 1987 A finite-element study of the onset of vortex shedding in flow past variously shaped bodies. *J. Fluid Mech.* **182**, 23–45.

JAYAWEERA, K. O. L. F. & MASON, B. J. 1965 The behaviour of freely falling cylinders and cones in a viscous fluid. *J. Fluid Mech.* **22**, 709–720.

JOSEPH, D. D., FORTES, A. F., LUNDGREN, T. S. & SINGH, P. 1987 Nonlinear mechanics of fluidization of beds of spheres, cylinders and disks in water. In *Advances in Multiphase Flow and Related Problems* (ed. G. Papanicolau), pp. 101–122. SIAM.

JOSEPH, D. D. & LUNDGREN, T. S. 1990 Ensemble averaged and mixture theory equations for incompressible fluid particle suspensions. *Intl J. Multiphase Flow* **16**, 35–42.

KIM, I., ELGHOBASHI, S. & SIRIGNANO, W. A. 1993 Three-dimensional flow over two spheres placed side by side. *J. Fluid Mech.* **246**, 465–488.

KIM, S. 1991 *Microhydrodynamics: Principles and Selected Applications.* Butterworth-Heinemann.

LAMB, H. 1932 *Hydrodynamics*, 6th edn. Cambridge University Press.

LEAL, L. G. 1980 Particle motion in a viscous fluid. *Ann. Rev. Fluid Mech.* **12**, 435–476.

LUGT, H. J. & HAUSSLING, H. J. 1974 Laminar flow past an abruptly accelerated elliptic cylinder at 45° incidence. *J. Fluid Mech.* **65**, 711–734.

MORKOVIN, M. V. 1964 Flow around circular cylinder – a kaleidoscope of challenging fluid phenomena. *ASME Symp. on Fully Separated Flows, Philadelphia, PA* (ed. A. G. Hansen), pp. 102–118.

NOMURA, T. & HUGHES, T. J. R. 1992 An arbitrary Lagrangian–Eulerian finite element method for interaction of fluid and a solid body. *Comput. Meth. Appl. Mech. Engng* **95**, 115–138.

OTA, T. & NISHIYAMA, H. 1984 Heat transfer and flow around an elliptic cylinder. *Intl J. Heat Mass Transfer* **27**, 1771–1779.

PARK, J. K., PARK, S. O. & HYUN, J. M. 1989 Flow regimes of unsteady laminar flow past a slender elliptic cylinder at incidence. *Intl J. Heat Fluid Flow* **10**, 311–317.

PATEL, V. A. 1981 Flow around the impulsively started elliptic cylinder at various angles of attack. *Computers Fluids* **9**, 435–462.

REPETTI, R. V. & LEONARD, E. F. 1966 Physical basis for the axial accumulation of red blood cells. *Chem. Engng Prog. Symp. Ser.* **62** (*no.* 66), 80–87.

SAFFMAN, P. G. 1956 On the rise of small air bubbles in water. *J. Fluid Mech.* **1**, 249–275.

SHINTANI, K., UMEMURA, A. & TAKANO, A. 1983 Low-Reynolds-number flow past an elliptic cylinder. *J. Fluid Mech.* **136**, 277–289.

SUCKER, D. & BRAUER, H. 1975 Fluiddynamik bei quer angeströmten Zylindern. *Wärme- und Stoffübertragung* **8**, 149–158.

TACHIBANA, M. 1973 On the behaviour of a sphere in the laminar tube flows. *Rheol. Acta* **12**, 58–69.

TANEDA, S. 1977 Visual study of unsteady separated flows around bodies. *Prog. Aerospace Sci.* **17**, 287–348.

THOM, A. 1933 The flows past circular cylinders at low speeds. *Proc. R. Soc. Lond.* A **141**, 651–669.

UNVERDI, S. O. & TRYGGVASON, G. 1992 A front-tracking method for viscous, incompressible, multi-fluid flows. *J. Comput. Phys.* **100**, 25–37.

VAN DYKE, M. 1982 *An Album of Fluid Motion.* Parabolic.

VASSEUR, P. & COX, R. G. 1977 The lateral migration of spherical particles sedimenting in a stagnant bounded fluid. *J. Fluid Mech.* **80**, 561–591.

VOLPICELLI, G., MASSIMILLA, L. & ZENZ, F. A. 1966 Nonhomogeneities in solid–liquid fluidization. *Chem. Engng Prog. Symp. Ser.* **62** (*no.* 67), 42–50.

WACHOLDER, E. & SATHER, N. F. 1974 The hydrodynamic interaction of two unequal spheres moving under gravity through quiescent viscous fluid. *J. Fluid Mech.* **65**, 417–437.

WILLIAMSON, C. H. K. 1988 Defining a universal and continuous Strouhal–Reynolds number relationship for the laminar vortex shedding of a circular cylinder. *Phys. Fluids* **31**, 2742–2744.